INVESTIGATING THE IMMEDIATE EFFECTS OF CONTROLLED SOCCER HEADERS ON EEG

by

Yi Lun Timothy Wang

B.E. (Hons), The University of Auckland, 2017

A THESIS SUBMITTED IN PARTIAL FULFILLMENT OF

THE REQUIREMENTS FOR THE DEGREE OF

MASTER OF APPLED SCIENCE

in

THE FACULTY OF GRADUATE AND POSTDOCTORAL STUDIES

(Biomedical Engineering)

THE UNIVERSITY OF BRITISH COLUMBIA

(Vancouver)

August 2020

The following individuals certify that they have read, and recommend to the Faculty of Graduate and Postdoctoral Studies for acceptance, a thesis entitled:

Investigating The Immediate Effects Of Controlled Soccer Headers On EEG

submitted by Yi Lun Timothy Wang in partial fulfillment of the requirements for

the degree of Master of Applied Science

in Biomedical Engineering

Examining Committee:

Lyndia Wu, Assistant Professor, Department of Mechanical Engineering, UBC
Supervisor

Peter Cripton, Professor, School of Biomedical Engineering, UBC
Supervisory Committee Member

Naznin Virji-Babul, Associate Professor, Department of Medicine, UBC
Supervisory Committee Member

Abstract

Soccer heading is a common technique where players use their head to pass, shoot or clear the ball. The ball-to-head impact involved in this technique has raised concern for risk of head and brain injury. However, there are inconclusive findings on the effect of soccer headers in the literature. The objective of this study was to investigate, in a controlled environment, whether mild soccer head impacts result in immediate neurophysiological changes in the brain, and if yes, whether the changes are affected by impact level and header direction. Controlled soccer headers were simulated at 2 impact levels in 3 directions, representative of the mildest headers experienced on the field, using a custom pendulum impactor with a soccer ball attachment. Participants were instrumented with an inertial measurement unit (IMU) to record the head kinematics of head impacts and an electroencephalography (EEG) device to measure neurophysiological changes. The EEG changes were evaluated by four metrics (absolute and relative power, magnitude squared and imaginary coherence) for common brain wave frequency bands. With data from 8 participants (6 males, 2 females), the study provided statistically significant evidence of the immediate neurophysiological changes after mild soccer headers. We found a surge in normalized absolute power right after heading across all the frequency bands with a larger increase for headers at the higher impact level. In addition, we observed an increase in delta band relative power, along with a decrease in the higher frequency bands, indicating slowing of activity in the brain. These findings are consistent with those observed in patients with traumatic brain injury or post-concussive syndrome. Aside from changes in power, we also found evidence of significant changes in coherence with different patterns between magnitude squared and imaginary coherence, suggesting effects of heading on the brain's functional connectivity. Finally, we found evidence that these changes diminished over time and participant's neurocognitive performance remained

unchanged. Our findings suggest that even mild soccer headers could lead to immediate, transient neurophysiological changes and highlight the importance of further investigation of the effects of long-term head impact accumulation in sports.

Lay Summary

This study investigated the immediate effects of soccer heading on the brain for different impact level and direction by looking at brain waves during an experiment. The participants in the experiment received soccer headers simulated with different impact levels and directions, and their brain waves were collected and analyzed to evaluate heading effects on the brain. Our results showed evidence of the immediate effects of heading on the brain, with the size of these effects associated with impact level and direction. The findings from this study suggested possible associations of soccer headers with mild transient brain changes, and a possible new approach for further research on the effects of sports head impacts.

Preface

The main contributors to the work presented in this thesis include me, a Mechanical Engineering Master's student Cyrus Titina, and our supervisor Dr. Lyndia Wu. The project was initiated by Dr. Wu, and all three of us were involved in the development of the experimental plan. We received research ethics approval for this study and obtained informed consent from all participants (UBC Clinical Research Ethics Board H19-00602).

For the experimental setup in Chapter 2, I was responsible for the EEG setup and Cyrus Titina for building and managing the pendulum impactor. I was also in charge of developing a time-synchronization mechanism to synchronize signals from all sensors with millisecond precision.

For experimental data collection, I was mostly responsible for conducting the experiments with the occasional help of Cyrus Titina, and other members of the SimPL lab.

For the data analysis, I was entirely responsible for the pre-processing and de-noising of the EEG signal. In addition, I was entirely in charge of performing power spectral analysis, coherence analysis, and recovery analysis presented in Chapters 3, 4 and 5 respectively.

The results presented in Chapters 3 and 4 were submitted in conference abstracts and accepted for presentation at the 2020 Summer Biomechanics, Bioengineering, and Biotransport Conference. A journal manuscript of the work presented in this thesis is under preparation.

Table of Contents

Abstract ..... **iii**

Lay Summary ..... **v**

Preface ..... **vi**

Table of Contents ..... **vii**

List of Tables ..... **x**

List of Figures ..... **xi**

List of Abbreviations ..... **xiv**

Acknowledgements ..... **xv**

Dedication ..... **xvi**

Chapter 1: Introduction **1**

1.1 Soccer Heading and Brain Injury 1

1.2 Brain Injury Effects on EEG 2

1.3 EEG Spectral Analysis 4

1.4 Coherence Analysis of EEG Signals 6

1.5 Objectives 9

Chapter 2: Experimental Methods **11**

2.1 Participants 11

2.2 Experiment Setup 11

2.2.1 Instrumentation Setup 11

2.2.2 Pendulum Soccer Impactor 13

2.2.3 Pretrial Experiment Setup 14

2.3 Protocol 15
2.4 Data Processing 16
2.5 Statistical Analysis 18
Chapter 3: Post-Impact Changes in EEG Power 21
3.1 Statistical Analysis of Power Data 21
3.2 Head Kinematic and EEG Results 22
3.3 Absolute Power Results 24
3.4 Relative Power Results 29
3.5 Discussion 34
Chapter 4: Post-Impact Changes in EEG Coherence 39
4.1 Functional Connectivity through Coherence Analysis 39
4.2 Statistical Analysis of Coherence Data 41
4.3 Magnitude Squared Coherence Results 42
4.4 Imaginary Coherence Results 47
4.5 Discussion 52
Chapter 5: EEG Recovery and Neuropsychological Evaluation 56
5.1 Post Impact Recovery 56
5.2 Post Session Recovery 58
Chapter 6: Conclusions 63
Bibliography 66
Appendix A: Pre- and Post-Heading Statistics with Loading Direction and Speed 70
Pre- and Post-Heading Statistics with loading direction and speed for Relative Power 70
Pre- and Post-heading Statistics with loading direction and speed for Absolute Power 71

Pre- and Post-heading Statistics with loading direction, speed and electrode group for Magnitude Squared Coherence 72

Pre- and Post-heading Statistics with loading direction, speed and electrode group for Magnitude Squared Coherence 77

Appendix B: Summary Statistics of the Data of Heading 82

List of Tables

Table 3.1 Regression analysis of absolute power with loading direction and speed 27

Table 3.2 Regression analysis of absolute power with a single factor 28

Table 3.3 Regression analysis of relative power with loading direction and speed 32

Table 3.4 Regression analysis of relative power with a single factor..... 32

Table 4.1 Classification of 19 electrodes according to their locations on a scalp map 40

Table 4.3 Regression analysis of magnitude squared coherence with loading direction, speed and electrode group..... 44

Table 4.3 Regression analysis of magnitude squared coherence with a single factor 46

Table 4.4 Regression analysis of imaginary coherence with loading direction, ball speed, and electrode group..... 50

Table 4.5 Regression analysis of imaginary coherence with a single factor 51

Table 6.1 Summary statistics of the whole data of change in absolute power from pre-heading to post-heading..... 82

Table 6.2 Summary statistics of the trimmed data of change in absolute power from pre-heading to post-heading..... 83

Table 6.3 Summary statistics of the data of change in relative power from pre-heading to post-heading..... 83

Table 6.4 Summary statistics of magnitude squared coherence data..... 83

Table 4.5 Summary statistics of imaginary coherence data..... 84

List of Figures

Figure 2.1 Sample Electrode locations on a scalp map 12

Figure 2.2 Pendulum setup in our experiment 13

Figure 3.1 The EEG data before applying ICA decomposition. 23

Figure 3.2 The EEG after applying ICA decomposition 23

Figure 3.3 Sample synchronized processed EEG, angular velocity magnitude and linear acceleration plot with the force peak in at time = 0. 24

Figure 3.4 Boxplot of change in absolute power from pre-heading to post-heading 25

Figure 3.5 Bar graphs of average change in absolute power from pre-heading to post-heading . 26

Figure 3.6 The average difference in the change of absolute power between shams and impacts29

Figure 3.7 Boxplot of change in relative power from pre-heading to post-heading 30

Figure 3.8 The average change in relative power from pre-heading to post-heading. 31

Figure 3.9 The average difference in the change of relative power between shams and impacts 33

Figure 3.10 The average change in absolute power from pre-heading to post-heading for three loading directions. 35

Figure 3.11 The average change in absolute power from pre-heading to post-heading for 4 rad/s and 7 rad/s 36

Figure 3.12 The average change in relative power from pre-heading to post-heading for three loading directions. 37

Figure 3.13 The average change in relative power from pre-heading to post-heading for 4 rad/s and 7 rad/s 38

Figure 4.1 Classification of coherence groups on the scalp map 40

Figure 4.2 Change in magnitude squared coherence from pre-heading to post-heading in alpha band for one participant for a 4 rad/s frontal impact 41
Figure 4.3 Boxplot of change in magnitude squared coherence from pre-heading to post-heading 43
Figure 4.4 The average change in magnitude squared coherence from pre-heading to post-heading. 44
Figure 4.5 The average change in magnitude squared coherence from pre-heading to post-heading for three loading directions. 45
Figure 4.6 The average difference in the change of magnitude squared coherence between shams and impacts. 47
Figure 4.7 Boxplot of change in imaginary coherence from pre-heading to post-heading 48
Figure 4.8 The average change in imaginary coherence between pre-heading and post-heading. 49
Figure 4.9 The average difference in the change of imaginary coherence between shams and impacts 52
Figure 4.10 The average change in magnitude squared coherence from pre-heading to post-heading for 4 rad/s and 7 rad/s. 54
Figure 4.11 The average change in magnitude squared coherence from pre-heading to post-heading for eight coherence groups. 54
Figure 5.1 The average change in absolute power from pre-heading to post-heading for 2-second and 5-second epochs. 57
Figure 5.2 The average change in relative power from pre-heading to post-heading for 2-second and 5-second epochs. 58
Figure 5.3 The average accuracy for the three sections of the concussion test after all the trials 59

Figure 5.4 The average difference in absolute power between post and pre resting states. 61

Figure 5.5 The average difference in relative power between pre-resting and post-resting states. 61

Figure 5.6 The average difference in magnitude squared coherence between pre- and post-resting states. 62

Figure 5.7 The average difference in imaginary coherence between post- and pre-resting states. 62

Figure 6.2 Boxplot of change in absolute power from pre-heading to post-heading for the whole data of absolute power 82

List of Abbreviations

ADHD - attention deficit-hyperactivity disorder

ANOVA – analysis of variance

CTE – chronic traumatic encephalography

EEG – electroencephalography

ICA – independent component analysis

IMU – inertial measurement unit

mTBI – mild traumatic brain injury

PCS – post concussive syndrome

SAC – standard assessment of concussion

SCAT5 – sport concussion assessment tool 5

TBI – traumatic brain injury

Acknowledgements

I wish to thank all the people who have supported and assisted me during my study at UBC. Particularly, I wish to express my deepest gratitude to my supervisor, Professor Lyndia Wu for guidance throughout the research project, which helped me to become a better researcher. I also wish to show my gratitude to Professor Peter Cripton and Professor Naznin Virji-Babul for advice and suggestions on the research, which helped me to improve my thesis tremendously.

There are many other people who have helped me along the way, especially my fellow students at UBC, Cyrus Titina and Derek Fong, and all the members of the SimPL lab at UBC. I offer my sincere thanks for your influence and assistance. This work would not have been possible without these support networks and I have been very fortunate to benefit from your expertise and friendship.

I also wish to thank for the financial support that I received from UBC, particularly the grant for the research project from Natural Sciences and Engineering Research Council of Canada (NSERC, RGPIN-2018-04606).

Special thanks are owed to my family, whose have supported me throughout my years of education.

Dedication

“There are no shortcuts to any place worth going.”

— Beverly Sills

Chapter 1: Introduction

Soccer is a popular and unique sport where players can use their heads purposefully for controlling the ball without any protection. According to a conservative estimate, there is an average of 6 headers per player during a game. Most soccer headers are mild and would result in mild average head accelerations of around 13g and 2000 rad/s^2 (Caccese et al. 2016). As cumulative sports head impacts may cause long term brain changes (Asken et al. 2017), soccer head impacts have raised a lot of concerns for potential long-term risk of soccer heading as noted in some medical guidelines, despite the absence of definitive evidence that soccer heading causes acute traumatic brain injury (TBI) (e.g., Patlak and Joy, 2002, Koutures and Gregory, 2010). Hence, it indicates the need for more studies investigating the effect of soccer head impacts on the brain, to prevent potential longer-term effects.

1.1 Soccer Heading and Brain Injury

In the literature, while many studies of heading effects attempt to establish the association of soccer headers with brain injury, the findings from these studies are inconclusive. For instance, several studies with data from professional European soccer players suggest that extended exposure to soccer may be associated with chronic cognitive impairment. Specifically, Tysvaer and Løchen (1991) found some degree of permanent brain damage in professional soccer players, which may be associated with repeated traumas from soccer heading. Matser et al. (1998) found that some cognitive impairments related to memory and planning were associated with the number of concussions incurred in soccer games and the frequency of soccer heading, which was derived based on the data from active professional soccer players from several professional Dutch soccer clubs compared with a control group of elite noncontact sport athletes. Master et al. (1999) also found that some cognitive impairments were associated with the combination of soccer-related

concussions and the number of headers based on the data from amateur soccer players with a control group of amateur athletes involved in swimming and track. However, there is opposing evidence from similar studies. For example, several studies in the literature found no significant evidence of the association between acute changes in postural control and routine soccer heading (Broglio et al. 2004), and no cognitive deficits due to repeated exposure to heading based on the data from US soccer players (Jordan et al. 1996, Guskiewicz et al. 2002).

Some studies applied EEG and other neuroimaging techniques to determine whether neurophysiological changes arise from soccer heading. For instance, Kross et al. (1983) examined soccer players' EEGs before and after heading training to determine whether soccer headers had any acute effects, but found no evidence of any EEG changes. Tysvaer et al. (1989) studied EEG recordings of retired soccer players and found no significant difference in the EEG between players that sustain more headers and the other soccer players as well as no differences between players reporting head trauma symptoms and those without symptoms. However, Tysvaer and Storli, (1989) also examined EEG data from professional soccer players and found evidence that EEG could sensitively detect neurophysiological abnormalities in soccer players compared with controls, likely due to a history of soccer brain injuries or accumulation of mild headers. Because of such inconclusive findings in prior literature, it is still unclear what effects individual soccer headers may have on the brain, and how such effects accumulate. It also suggests the need for exploring different ways to investigate head impacts.

1.2 Brain Injury Effects on EEG

EEG signals from different electrodes record the potential differences in electrical activities in the brain between different electrode locations on the scalp with one of them chosen as a reference electrode for comparison (Olenjniczak, 2006). While there are various electrical

activities in the brain, including those with action potentials and post-synaptic potentials, EEG signals can only effectively record the ones having enough duration and amplitude. Specifically, EEG can properly record summed post-synaptic potentials as they meet the conditions of duration and amplitude.

Since the electrical activity of neurons in the brain produces currents that reach the surface of the scalp, the use of EEG signals from electrodes on the scalp is a non-invasive method of recording the voltage differences of these scalp potentials. EEG also directly measures the biophysical phenomena at the level of populations of neurons, which has an advantage over other non-invasive methods that use functional measures based on MRI that gauge hemodynamic responses instead of neural activities (Singh 2012). Moreover, EEG is multidimensional with EEG analysis applied to not only time and space domains, but also frequency, power and phase. This allows more flexibility in the analysis of neural dynamics as compared with other non-invasive methods. Thus, EEG is widely used as a test that detects abnormalities in brain waves, or in the electrical activity of brain in both medical practice and academic research. For example, EEG is used to examine awareness in patients with severe brain injury (Bai et al., 2008), to evaluate the clinical presentation and pathophysiology of mild TBI (Nuwer et al., 2005), and to analyze the persistent functional deficits in athletes suffering from mild TBI (Thompson et al., 2005). More specifically, Nuwer (2005) provided the detailed review and discussion about how EEG has been used as a clinical diagnostic test to identify, confirm, measure and localize brain injury among mild TBI patients. The study by Thompson (2005) attempted to identify long-lasting abnormal trends of EEG patterns in isolation and those associated with various degrees of challenge in postural tasks in individuals suffering from mild TBI. It provided evidence of a decrease in EEG power in all the frequency bands studied with twelve athletes suffering from mild TBI, especially

in standing postures. It also showed presence of long-term functional abnormalities in individuals suffering from mild TBI.

There are several advantages to applying EEG in brain injury studies. In clinical practice, EEG is a relatively low-cost approach that enables multiple testing sessions for different states of arousal. EEG signal can also be gathered at high sampling rates, typically offering millisecond-level temporal resolution, which enables capturing potentially transient changes and fast dynamics in the brain. Finally, EEG is an established method that has been used to examine cognitive processes via a neuropsychological approach (O'Gormon). It is known that one of the major outcomes of brain injury is neurocognitive deficit, hence EEG can be used to investigate deeper into the source of neurocognitive changes from brain injury.

1.3 EEG Spectral Analysis

EEG spectral analysis is a basic type of EEG analysis that quantifies the amount of rhythmic or oscillatory activity of different frequency EEGs, which was first developed by several pioneers in the 1800's (Coenen et al., 2014). The key objective of spectral analysis is the determination of the power spectrum density (power spectrum) of EEG signal from an electrode, which can be estimated by using the Welch periodogram estimate (Welch,1967) within each frequency band and the epochs windowed with a Hann window of a resolution of 0.5Hz. The Welch's estimation formula is expressed by

$$\hat{S}_x^W(\omega_k) = \frac{1}{K}\sum_{i=1}^{n} P_{X_m,M}(\omega_k),$$

where K is the total number of blocks in an EEG signal, and $P_{X_m,M}(\omega_k)$ is the periodogram of the M^{th} block, defined as the square-magnitude discrete time Fourier transform of the signal ($FFT_{N,k(x_m)}$) as follows:

$$P_{X_m,M}(\omega) = \frac{1}{M} | FFT_{N,k(x_m)} |^2 .$$

It is worth noting that the Welch's estimate usually has high accuracy and low variance when it is used over the classic periodogram, but it has low frequency resolution. In addition, the Welch's estimate of EEG power spectral density requires dividing the EEG signal into blocks and averaging the periodograms over each block.

The estimated EEG power spectrum is then used to assess the level of activity over multiple frequencies of EEG signals, usually within a narrow frequency band. While there are some small variations in the classification of different frequency band boundaries for EEG spectral analysis among different studies in the literature, the commonly used frequency bands in the literature are defined as follows: delta (1.0–4.0 Hz), theta (4.0–7.0 Hz), alpha (7–13 Hz), beta (13–22 Hz) and gamma (22–40 Hz) (e.g., Thatcher et al, 1989; Thatcher, 2010; Slobounov et al, 2012). As surveyed by Newson and Tiagarajan (2019), a total of 184 publications in PubMed published between 1993 and 2018 have used these pre-defined frequency bands in EEG power spectrum for various studies on brain impairments. As many studies in the literature have found that different brain impairments exhibit different characteristic patterns in each of these pre-defined frequency bands (e.g., Newson and Tiagarajan, 2019); the use of these pre-defined frequency bands allowed us to compare the changes in each frequency band from our study with those from previous studies in the literature. Consequently, we used these five frequency bands for EEG spectral analysis in our study.

There are two common methods to represent the estimated EEG power spectrum in the literature: namely absolute power and relative power. The former calculates the mean power in an EEG signal over a given frequency band as the absolute power of the signal for that frequency

band by the integral of the EEG power spectral density over the frequency band. The latter calculates the ratio of the absolute power of an EEG signal for a given frequency band to the absolute power of the signal over all bands as the relative power of the signal for the frequency band. We used both absolute and relative power in our study. This is because the absolute power and relative power allow us to examine change in the total power of an EEG signal in a frequency band and in the proportion of the total power of an EEG signal in a frequency band relative to the total power over all the frequency bands respectively. The 184 publications reviewed by Newson and Tiagarajan (2019) have used absolute and relative power in different studies on various brain impairments including depression, attention deficit-hyperactivity disorder (ADHD), and schizophrenia.

1.4 Coherence Analysis of EEG Signals

The human brain is a vast network of connected pathways that communicate through synchronized electric brain activity along fiber tracts. Brain connectivity describes the networks of functional and anatomical connections across the brain. Functional connectivity is defined as the measure of coupling strength through statistical analysis such as correlation and spectral coherence between two signals obtained from electrodes (Uddin, 2013). As reviewed in Bowyer (2016), well-connected highly synchronous functional activity can be measured by EEG and then analyzed with several types of mathematical methods. Particularly, coherence is one of such mathematical methods that can be used to determine whether two or more EEG electrodes have similar neuronal oscillatory activity with each other. Coherence analysis of EEG signals based on EEG spectral density can be used to extract transient characteristics of interactions among brain areas and examine coordination of EEG rhythms between brain areas. The aim of coherence analysis of EEG signals is to describe the temporal, spatial and frequency relationships of brain

activities. While there have been many different measures and methods in the literature to quantify the brain's functional connectivity with different types of data, we adopted two commonly used coherence-based metrics for function connectivity in our study: (1) magnitude squared coherence and (2) imaginary coherence. This is because the use of both measures has been shown to be very useful in the analysis of functional connectivity (Sander et al., 2010).

As defined in Nolte et al. (2004), coherence between two electrodes is a measure of the correlation, represented by the cross-spectrum, between the signals recorded from the two electrodes at a specific frequency that has been normalized by the product of the power of the two signals. Specifically, let $x_i(f)$ and $x_j(f)$ be the Fourier transformation of the time series $\hat{x}_i(f)$ and $\hat{x}_j(f)$ of signals from electrodes *i* and *j* respectively. The cross-spectrum is then defined as

$$S_{ij}(f) \equiv \left\langle x_i(f) x_j^*(f) \right\rangle, \tag{1}$$

where * stands for complex conjugation and $\langle . \rangle$ for expectation value that is estimated as an average over a sufficiently large number of epochs. The normalized cross-spectrum is used to measure the strength of the linear relationship in EEG signal between two electrodes i and j and denoted by

$$C_{ij}(f) = \frac{S_{ij}(f)}{\sqrt{S_{ii}(f) S_{jj}(f)}}. \tag{2}$$

$C_{ij}(f)$ can be split into real and imaginary parts and different quantities can be analyzed further. Particularly, magnitude squared coherence is defined as the modulus of $C_{ij}(f)$ as follows:

$$MC_{ij}(f) = \frac{\left|S_{ij}(f)\right|^2}{\sqrt{S_{ii}(f) S_{jj}(f)}}, \tag{3}$$

where $\left|S_{ij}(f)\right|$ stands for the magnitude of the spectral density. In addition, imaginary coherence is defined by the imaginary part of $C_{ij}(f)$, denoted as $IC_{ij}(f)$.

The magnitude squared coherence is bounded between 0 and 1, where 1 indicates a perfect linear prediction of the signal process i from knowledge of the signal process j. An increase in the magnitude squared coherence between EEG signals recorded at different electrodes indicates an increased functional connectivity between the neuronal networks (Oldrich et al., 2014). Consequently, it has been applied in many different studies, which, for example, includes the analysis of the cortical connection of Alzheimer patients (Ho et al., 2014), and the examination of complex cognitive functions for memory, language, and emotion (Vladimir and Andreas, 2015).

However, volume conduction is one of possible issues for the use of magnitude squared coherence in the analysis of the brain's function connectivity because of the effects of instantaneous correlations, i.e., the value of $MC_{ij}(f)$ would artificially increase when the same brain signal is detected by two adjacent electrodes. As such, Nolte et al. (2004) showed that the use of the imaginary coherence $IC_{ij}(f)$ can circumvent possible volume conduction in the estimation of functional connectivity, and improve the analysis of the brain's functional connectivity as compared with the use of magnitude squared coherence (Nolte, 2004). This is because the imaginary part of $C_{ij}(f)$ is insensitive to self-interaction caused by volume conduction since a signal cannot be time-lagged to itself.

It is worth noting that when the value of $IC_{ij}(f)$ is small or negligible, it does not necessarily mean that there is no presence of a significant interaction between EEG signals in some cases. For instance, if the phase difference between two EEG signals from two electrodes is near zero, the

value of $IC_{ij}(f)$ is likely close to zero regardless whether there is a true interaction between the two signals. Clearly, it is important to analyze the brain's functional connectivity based on both $MC_{ij}(f)$ and $IC_{ij}(f)$. Hence, we use both measures to evaluate changes in coherence due to soccer headers in this study.

1.5 Objectives

Prior studies have found conflicting results regarding the potential neurological and neurophysiological effects of soccer heading. However, there are several general limitations in these studies including the lack of baseline measurements, the limited resolution to examine the effects of individual headers, and the delayed time of testing where transient and subtle effects may not be captured. We still anticipate that even mild head impacts may lead to mild and transient electrophysiological changes, since such impacts are estimated to lead to brain deformations and axonal loading based on computational modeling (Miller, 2019). One main challenge is to determine whether and how potential transient effects of mild soccer headers can be measured sensitively and quantitatively. In the current thesis, we tackled this challenge by conducting a novel set of experiments to continuously measure EEG activity during a bout of soccer head impacts. The main research questions are: can the immediate effects of a mild soccer header on the brain be detected with the use of EEG, and are these effects affected by header direction and ball speed? In this study, we conducted controlled soccer headers at 2 impact levels and in 3 header directions by a pendulum impactor with a soccer ball attachment. The impact levels represent the mildest headers experienced on the field. Participants were instrumented with an Inertial Motion Unit (IMU) on a custom-fit mouthguard to record the head kinematics of the soccer headers and an EEG device to measure possible neurophysiological changes. This investigation approach allows

us to directly measure neurophysiological changes of individual soccer head impacts with the use of continuous measurements of EEG as well as examine potential cumulative effects from a bout of head impacts in a controlled setting.

The rest of thesis is organized as follows. Chapter 2 describes the experimental methods. Chapters 3 and 4 present the results of post-impact changes in power and coherence, respectively. Chapter 5 describes the analysis of neurocognitive evaluation and EEG recovery. Finally, Chapter 6 presents our conclusions.

Chapter 2: Experimental Methods

2.1 Participants

We have recruited 8 participants (6 males and 2 females) for this study. The participants were healthy individuals between the age of 18 and 30, with at least 1 year of prior experience with soccer. An individual is ineligible to participate in our study given any of the following six exclusion criteria: (1) a recent history of head, neck or whiplash injury, (2) a diagnosed concussion history, (3) a neurological or spinal illness, (4) being pregnant, (5) head or neck pains, and (6) unable to provide informed consent. For the eight participants in our study, the average weight is 76.58 kg with standard deviation of 14.66 kg, and the average height is 1.67 m with standard deviation of 0.06 m respectively.

The human participant protocol for the recruitment of our study was approved by the UBC Research Ethics Board (H19-00602) and informed consent was obtained from all the participants.

2.2 Experiment Setup

2.2.1 Instrumentation Setup

The EEG amplifier used in our experiment is the ANT Neuro Refa System. We used the 10-20 electrode setup with reusable wet gold cup electrodes mounted at 19 scalp locations across the head, with EEG continuously sampled at 2048Hz throughout the experiment. We have chosen to use the 10-20 setup as it is widely used throughout the literature, especially for exploratory studies (Homan, 1987). We used linked earlobe electrodes as the reference, since it allows us to retain all 19 electrodes for analysis instead of sacrificing an electrode to be used as the reference. Dry electrodes are not attached to the scalp, hence they are not suitable for this experiment as they have a higher chance of electrode displacement with respect to the scalp upon the head impact. Since we used passive electrodes for this study, we had to ensure that the electrode impedances were

below 5kOhms. A scalp map showing the electrode locations is given in Figure 2.1 and with the 19 electrodes in Figure 2.1. The ground electrode is located between Fp1 and Fp2.

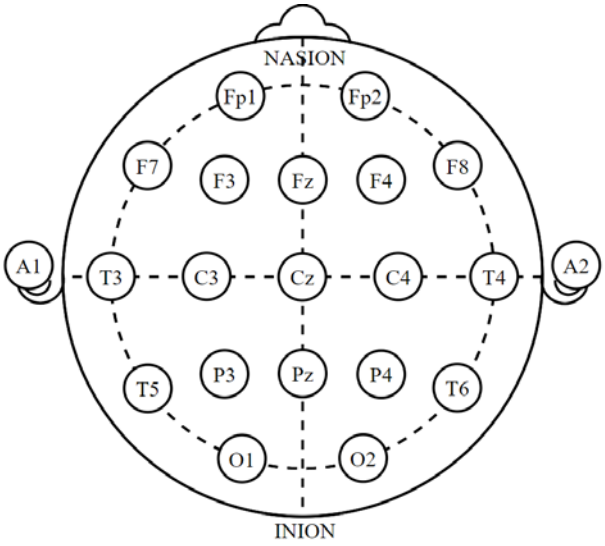

Figure 2.1 Sample Electrode locations on a scalp map

A load cell (Precision Technologies Model ST50) is used in our experiment to measure the force of the impact and to ascertain the exact time at which the impact occurred. The load cell has a sampling rate of 1kHz, a maximum loading capacity of 50 kg. The average forces observed in our study was around 230N for the low impact level and 360N for the high impact level with standard deviations of 62N and 72N for the two impact levels respectively.

An IMU, specifically the MPU6050 from TDK InvenSense, is attached onto a bitebar affixed to a mouthguard that is custom-formed, using a dental vacuum former, to each participant's upper dentition mold and worn by the participant during the trials. The IMU has a sampling rate of 1kHz and has a range of up to ±16G of linear acceleration and up to 2000 degrees/s (or 35 rad/s) of rotational velocity.

In summary, this experiment involves three sensors: the EEG amplifier, the force meter and the IMU. In order to synchronize the inputs received from each sensor, a syncing signal is sent to

all 3 sensors as an input. The syncing signal is a square wave with a frequency of 1Hz and an amplitude of 1 V that lasts for 8 seconds, which is sent right before an impact occurs and stops after the impact, allowing for sensor data synchronization with millisecond precision. The syncing signal is also used to simplify data processing by marking the impact times in all 3 sensors.

2.2.2 Pendulum Soccer Impactor

We have setup a pendulum impactor that is used to simulate soccer headers as shown in Figure 2.2. A soccer ball with a pressure of 10 psi is attached to the end of the impactor and the effective mass is around 10 kg. This setup can allow for adjustment of the input force from the soccer impact by changing the pendulum angle. A ratcheting system is added to the impactor to prevent multiple impacts by stopping the pendulum arm after initial impact. For our experiment, we tuned the pendulum set up for two impact levels, with peak resultant head linear acceleration of approximately 6-7g and peak head rotational velocity of approximately 4-5 rad/s for the lower level, and linear acceleration of 9-10g and rotational velocity of 7-8 rad/s at the higher level.

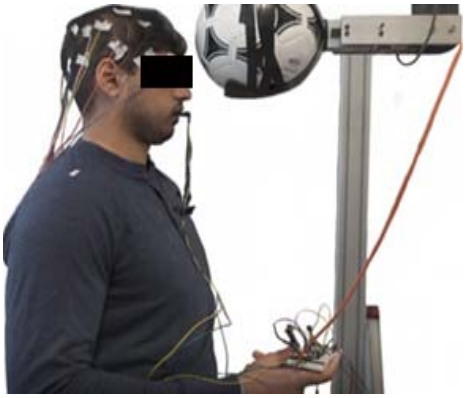

Figure 2.2 Pendulum setup in our experiment

In order to have repeatable head kinematics among participants and across different loading directions, we had to vary the pendulum angle for each participant to account for weight and height of individual participants. This was required as the greater the head mass, the lower the expected

head kinematics; the height of the participant may affect the moment arm as the pendulum height may need to be adjusted in order for the soccer ball attachment to hit the participant's forehead. Moreover, Kuo (2018) showed that coronal head impacts result in lower kinematics than in sagittal head impacts. This means that the same pendulum angle could result in different head rotational velocity for the side impacts as compared to the frontal impact. Thus, we conducted a pretrial experiment to establish an empirical relationship between the expected head kinematics based on the mass and height of an individual participant to account for the difference between coronal and sagittal head impacts. Based on this empirical relationship derived from the pretrial experiment, we tuned the pendulum angle for each participant to archive the targeted head kinematics across different loading direction.

2.2.3 Pretrial Experiment Setup

The pretrial experiment involves performing 3 headers in 3 different loading directions (front, oblique left and oblique right) and at 6 different pendulum angles (15º, 20º, 25º, 30º, 35º, 40º) for 2 male participants with different mass and height. The average angular velocity of the 3 headers in each heading scenario was plotted against the pendulum heights and a linear equation that related pendulum height with angular velocity was estimated using simple linear regression.

With this estimated regression equation, we then estimated the pendulum height at which the average angular velocity was set at around 4 rad/s and 7 rad/s for the 2 participants and used these heights to estimate another linear equation of pendulum height with the product of the participants' mass and height using simple linear regression. With the second estimated equation, we predicted pendulum angles used for individual participants in our experiment according to the product of individual's mass and height. These angles range between around 15º and 45º.

2.3 Protocol

On the day of the trials, each participant is first asked to complete a neurocognitive test battery, the Standard Assessment of Concussion (SAC) (McCrea, 2001), before the start of all the trials for the participant. The main objective of these tests is to check the participant's baseline level of short-term memory retention, concentration and orientation. After that, the participant is instrumented by attaching the electrodes onto the participant's scalp in the 10-20 format and asked to wear the bite bar with the IMU.

Prior to the trials, we also gather 5 minutes of resting state EEG measurements, during which the participant stares straight ahead and keep their head still. After recording the resting state measurements, we performed head impact trials at 3 different directions: one frontal and 2 side headers (left and right), at the 2 different pendulum angles achieving the two kinematics levels.

For each trial, the participant is instructed to be prepared for a frontal impact with a 3-second countdown given before the impact. All the participants are asked to tense their neck muscles for readiness of the coming impact. This reduces risks of potential injury due to unanticipated impacts. In addition, as pointed out in Cantu (1992), tensing neck muscles for the coming impact simulates the situation where soccer headers are usually done by soccer players.

The side headers are oblique frontal headers, with the oblique direction from the anterior-posterior direction, impacting the side of the frontal bone. Our choice of the oblique direction for side headers rather than 90 degrees from the anterior-posterior direction is because this is closer to how soccer headers are performed by soccer players based off multiple soccer heading guides. During the frontal header trials, 3 sham headers are randomly dispersed among the frontal headers. The purpose of the use of shams in the trials is to differentiate the changes in the EEG due to heading from that due to the participant being aware of the impending impact.

Immediately after all the trials, there is another rest period of 5 minutes, during which the resting state EEG is recorded again, while the participant stares straight ahead at the ball. After that, the participant undergoes the SAC of the SCAT-5 test again to assess their neurocognitive state after the experiment.

2.4 Data Processing

The data of EEG signals collected from our experiment are processed in MATLAB 2019a, with the EEGLAB toolbox (Delorme et al, 2004) mainly used for data preprocessing. The two steps in signal preprocessing in our study are (1) to synchronize the head impacts with the change in EEG signals from the electrodes and the angular velocity recorded by the IMU as much as possible, and (2) to perform filtering and remove artifacts in EEG signals (e.g. eye blinks, muscle activity) which may distort the analysis of head impact effects.

After preprocessing, to analyze the immediate effects of heading, we compared a 2-second-long epoch immediately after the head impact with an equal-length epoch prior to this head impact (henceforth referred to as the post-impact epoch and pre-impact epoch respectively). The choice of the use of a 2-second-long epoch for measuring immediate impact for our main findings was in consideration of the balance between capturing transient effects on the impact and maintaining sufficient frequency resolution for the lower frequency bands. In addition, 5 second epochs were also analyzed to examine any recovery of the EEG changes post-impact. To make these 2 and 5-second-long epochs, the EEG data from the full experiment were first split into multiple 20-second long epochs centered around the time point when the angular velocity magnitude reached its peak from the head impact. Then, we determined when the head stops moving post-impact by applying a threshold of 0.2 rad/s. This was used to define the start of the post-impact epoch. These 20-second long epochs were then split into the aforementioned 2 and 5-second-long epochs. The pre-

impact epoch starts at the beginning of the original 20-second long epoch in order to remove possible effects due to the participant receiving verbal instructions alerting of the impact. The post-impact epoch starts immediately after the head stops moving or after the observable slow-moving transients in the EEG trace subsides so that we minimize potential motion artifacts from the head impact movements. All the pre- and post-impact epochs were put into EEGLAB for further data processing and filtered to remove slow motion artifacts (0 to 1Hz noise) and the 60Hz power line noise.

We applied a 4^{th} order IIR Notch-filter for the EEG data at 60 Hz to remove line noise and then applied a high-pass filter for the filtered data at 1Hz to remove the DC offset. Furthermore, we used the Runica algorithm, the default Independent Component Analysis (ICA) decomposition algorithm in EEGLAB for ICA, to remove noise in EEG data due to blinks and muscle contraction, which displays each independent component identified with possible sources such as brain, muscle, heart, and line noise together with the corresponding probability for each source expressed by a percentage. Note that the 20-second epochs of EEG signals from all the trials for a participant were first grouped into 6 groups for the participant according to 2 impact levels and 3 loading directions with an additional group of 20-second epochs for shams, and then the ICA was applied to each of these epoch groups for each participant. We chose to reject a noise component identified as muscle or line noise or heart if its probability exceeds 70%. Finally, we visually verified the remaining components to see if there was any presence of blink-like or muscle-like characteristics in the processed EEG data. Epochs of the same impact level and loading direction for each participant were processed at the same time.

For the processed EEG data, we employed the Welch periodogram estimate (Welch,1967) within each frequency band using Matlab's 'pwelch' function and the epochs windowed with a

Hann window of a resolution of 0.5Hz in EEGLAB to obtain the estimated power spectrum density (power spectrum) of EEG signal from an electrode (Aziezah, 2020). The estimated EEG power spectrum is then used to assess the level of activity over multiple frequencies of EEG signals, usually within a narrow frequency band. We used the commonly used five frequency bands in the literature are defined as follows: delta (1.0–4.0 Hz), theta (4.0–8.0 Hz), alpha (8–12 Hz), beta (13–22 Hz) and gamma (22–40 Hz) in our study. The band power was calculated in Matlab using the 'bandpower' function.

We used both absolute and relative power to represent the estimated EEG power spectrum in our study. The former calculates the mean power in an EEG signal over a given frequency band as the absolute power of the signal for that frequency band by the integral of the EEG power spectral density over the frequency band. The latter calculates the ratio of the absolute power of an EEG signal for a given frequency band to the absolute power of the signal over all bands as the relative power of the signal for the frequency band. Both were calculated using Matlab's 'bandpower' function in the Signal Processing toolbox. The use of both absolute and relative power allows us to examine change in the total power of an EEG signal in a frequency band and in the proportion of the total power of an EEG signal in a frequency band relative to the total power over all the frequency bands, respectively.

2.5 Statistical Analysis

To evaluate the immediate neurophysiological changes after heading, we considered the changes in each of the four metrics (absolute power, relative power, magnitude squared coherence and imaginary coherence) between pre-heading and post-heading, between shams and hits, and between pre- and post-session resting state measurements respectively. Note that to control possible variation in absolute power due to different conditions of individual participants in our

experiment, we further scaled the difference in absolute power between pre-heading and post-heading and between shams and hits by normalising it by the absolute power of pre-resting power for each individual. As we conducted several trials for each impact of loading direction and ball speed on a participant in our experiment, there were repeated observations of a metric over time for each impact on a participant. For each of the four metrics, we calculated the average of the repeated observations of a metric for an impact on a participant and used it as an observation of the metric for the impact on the participant in the data for our study.

For each of the four metrics, we first conducted a paired t-test with the null hypothesis of no change in a metric due to heading to determine whether there is evidence of a significant change in that metric between pre-heading and post-heading for each of the five frequency bands. The evidence from the paired t-test addressed the key research question on whether mild soccer head impacts result in immediate neurophysiological changes in the brain.

We then conducted a F-test based on either two-way or three-way analysis of variance (ANOVA) with the first two factors or all the three factors representing header direction, ball speed, and electrode location respectively, to determine whether there is significant evidence that change in a metric due to heading is associated with the two or three factors for each of the five frequency bands. Note that the null hypothesis of the F-test for two- or three-way ANOVA is that the mean change in a metric due to heading is the same for all the factors against the alternative that the mean change in that metric due to heading is not the same for these factors. In addition, we conducted one-way ANOVA with each of the three factors separately to determine whether there is significant evidence that change in a metric due to heading varies over different levels of that factor. The null hypothesis of the F-test for one-way ANOVA is that the mean change due to heading is the same for all the levels of a factor with the alternative that the mean change due to

heading is not the same for all the levels of a factor. The evidence from the F-test of the three-way or one-way ANOVA addressed the other key research question on whether and how the immediate neurophysiological changes due to heading are affected by impact level and header direction.

Furthermore, for each of the four metrics, we conducted a t-test with the null hypothesis of no difference in a metric between shams and impacts in the front loading and either soft or hard ball speed (henceforth referred to their angular velocities of 4 rad/s and 7 rad/s respectively) to determine whether there is significant evidence of difference in that metric between shams and impacts for each frequency band. Lastly, we conducted a paired t-test with the null hypothesis of no change in a metric between the pre-resting state and post-resting state to determine whether there is evidence of a significant change in that metric between the two resting states.

In order to assess the statistical significance of the results, we have applied the Bonferroni correction to correct for the inflated Type 1 error due to having multiple comparisons.

Chapter 3: Post-Impact Changes in EEG Power

EEG power spectral analysis has been applied to assess the brain activity changes weeks after head impacts (Barr, 2011). In this chapter, we present detailed analysis methods and results for the changes in EEG absolute and relative power after head impacts.

3.1 Statistical Analysis of Power Data

With the processed EEG data for our study, we first carried out statistical analysis of power data by conducting a paired t-test for overall change in absolute or relative power to evaluate the overall neurophysiological change due to heading for each frequency band. We then conducted two-way ANOVA with loading direction (F1) and impact level (F2) to analyze the association of the change in relative or absolute power due to heading with the two factors, which can be expressed by the regression of the change in relative or absolute power (y_i) on the two factors as follows:

$$y_i = \beta_0 + \beta_1 F_{1,i} + \beta_2 F_{2,i} + \varepsilon_i. \qquad (4)$$

Note that F1 represents three loading directions: front, left, and right and F2 two impact level: 4 rad/s and 7 rad/s respectively. In addition, we conducted one-way ANOVA with a single factor separately to analyze the relationship between the change in relative or absolute power and different levels of the factor. The statistical tests performed here has been summarized in Chapter 2.5.

For the statistical analysis of power data, we also addressed the issue of possible inflated Type I error in multiple analyses on the same data by performing the Bonferroni correction. The threshold based on the Bonferroni correction with 16 tests for power data was 0.0031, which controls the overall probability of Type I error for all the statistical inferences within 0.05.

3.2 Head Kinematic and EEG Results

The low level impacts had a mean linear acceleration of 7g with a standard deviation of 1.4g, an angular velocity of 4.88 rad/s with a standard deviation of 1.27 rad/s and an angular acceleration of 928 rad/s^2 with a standard deviation of 465 rad/s^2. The high level impacts had a mean linear acceleration of 100G with a standard deviation of 1.9g, an angular velocity of 8.29 rad/s with a standard deviation of 1.87 rad/s and an angular acceleration of 1331 rad/s^2 with a standard deviation of 938 rad/s^2.

In the EEG signal, as circled in Figure 3.1, there were visible spikes in the Fp1 and Fp2 channels before ICA decomposition was applied, which were removed after ICA as shown in Figure 3.2. It is worth noting that while ICA decomposition was also applied to remove eye saccades in our study, such an effect of ICA decomposition was not easy to display in a time series plot. In addition, both Figures 3.1 and 3.2 did not display any noticeable pattern for presence of muscle artefacts in the EEG data.

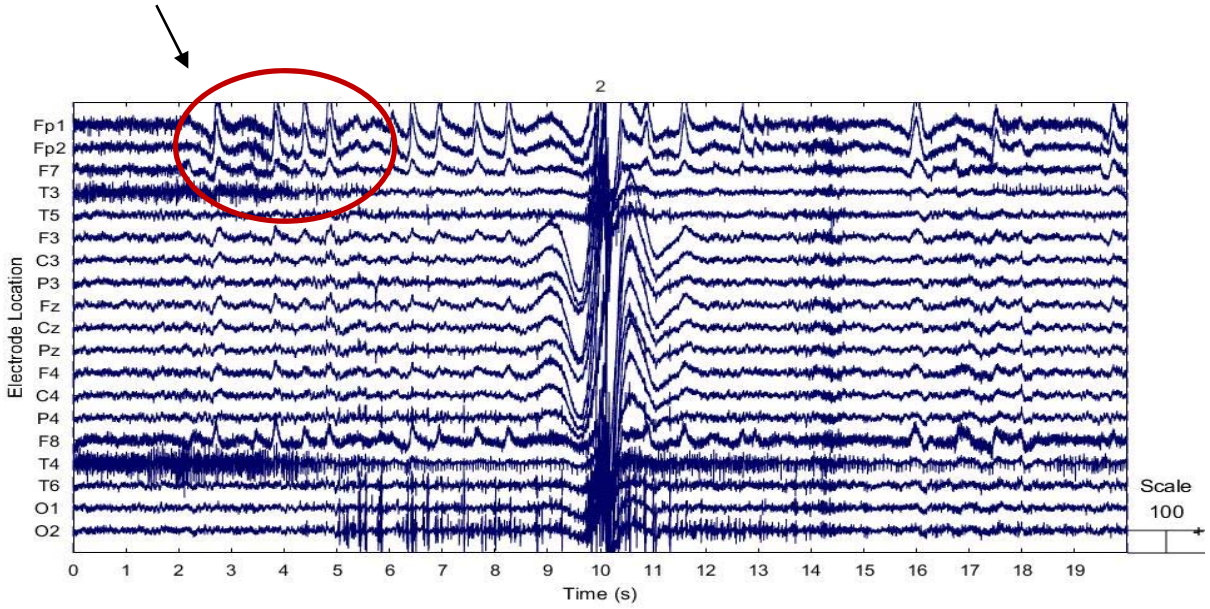

Figure 3.1 The EEG data before applying ICA decomposition.

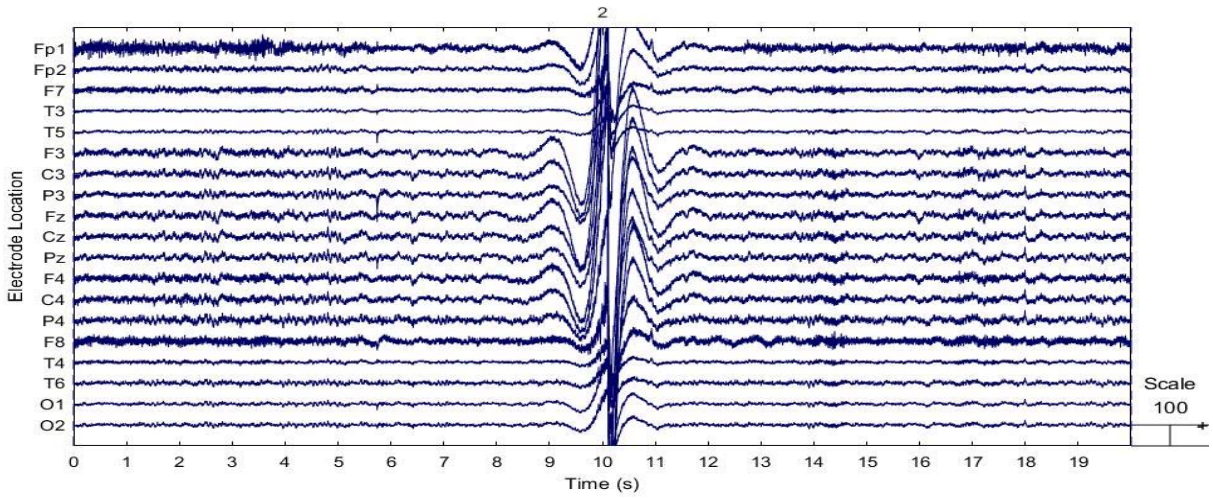

Figure 3.2 The EEG after applying ICA decomposition

As stated in Section 2.4, the EEG epochs with the kinematics and force were synchronized consistently before deriving the pre- and post-impact epochs in EEGLAB. The plots in Figure 3.3 display an example of a high-level impact where the peak in the angular velocity is situated at time 0 and the corresponding linear acceleration and processed EEG from the Fp2 electrode.

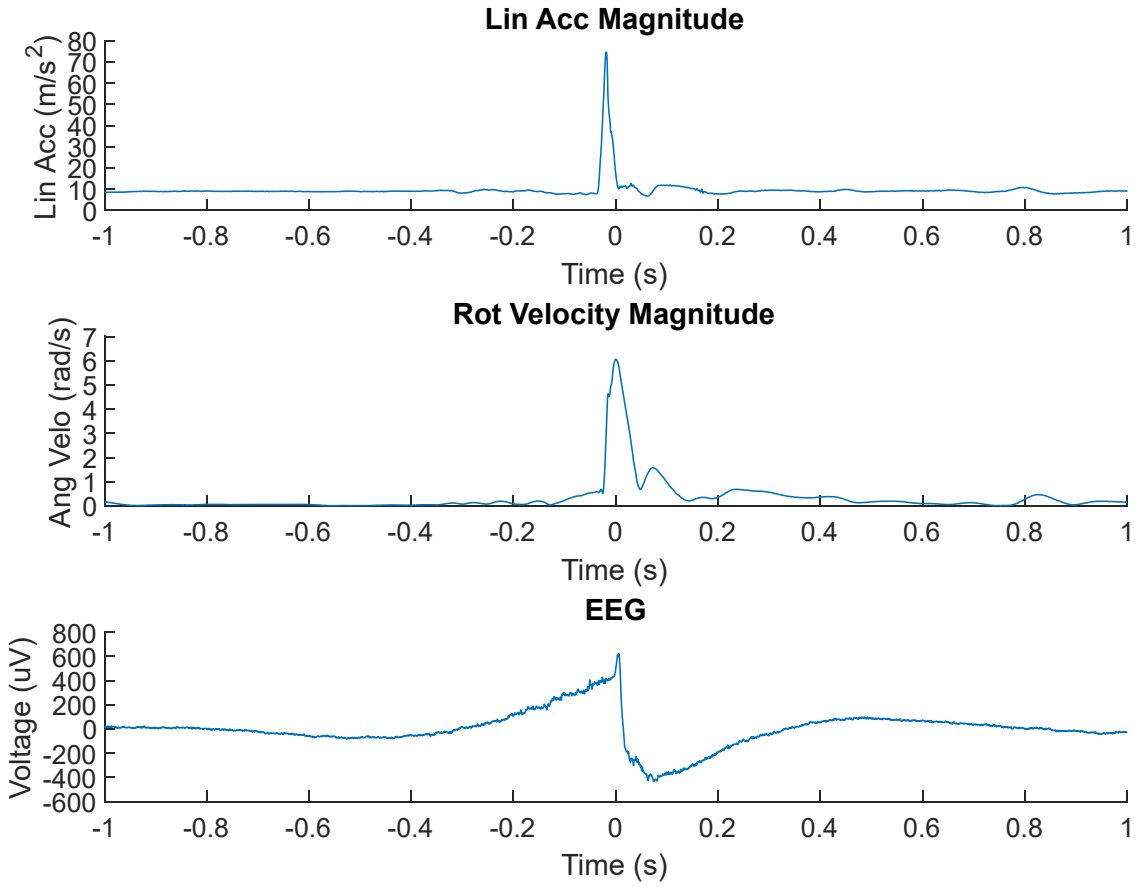

Figure 3.3 Sample synchronized processed EEG, angular velocity magnitude and linear acceleration plot with the force peak in at time = 0.

3.3 Absolute Power Results

We first analyzed the change in absolute power between the post-heading and pre-heading and found that there were some observations that were beyond normal physiological ranges of

EEG values, possibly due to static discharge, which is shown in Appendix B. Since the maximum physiological amplitude of EEG signals which are observed from epileptic seizures can go up to 1000 μV (Acharya et al. 2013), we excluded some of the extreme values in absolute power data that were derived from signals with an amplitude larger than 1000 μV. The boxplot of the trimmed data of change in absolute power from pre-heading to post-heading is presented in Figures 3.4 with the summary statistics of the trimmed data given in Appendix B. Overall, the data seem to be right skewed for all bands, i.e. skewed towards increases in absolute power. The change in the bands range from -109.2 to 399.9, and the average change in absolute power is 9.76 for Delta, 1.20 for Theta, 0.98 for Alpha, 6.62 for Beta, 0.99 for Gamma and 5.52 for the Total band.

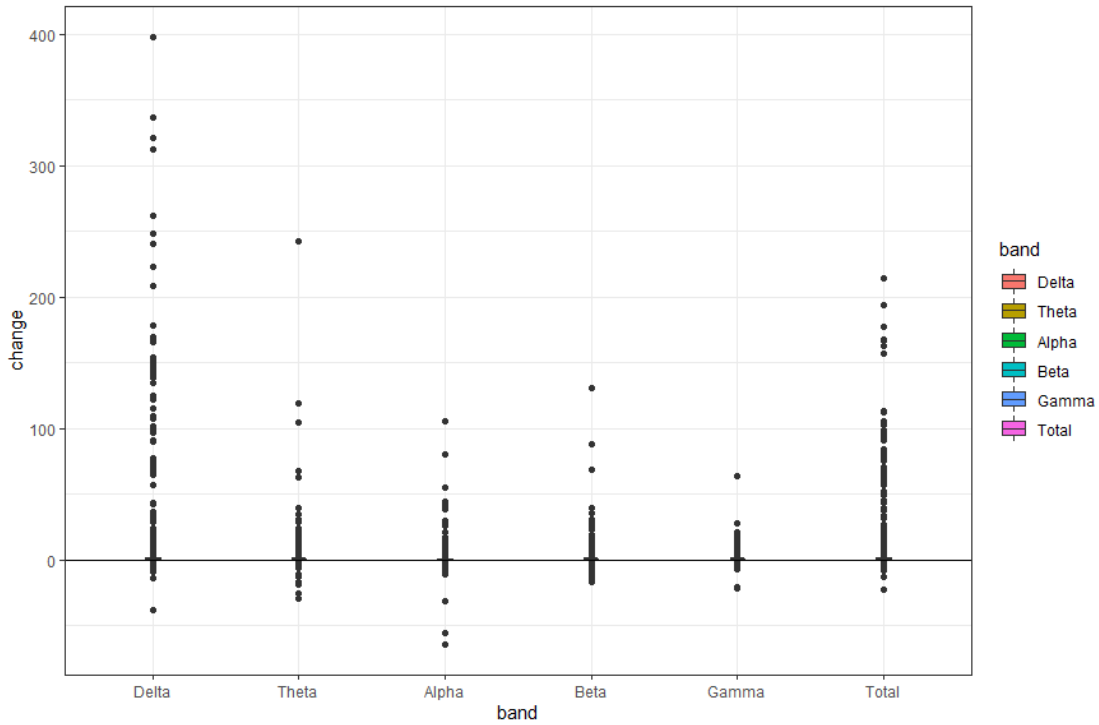

Figure 3.4 Boxplot of change in absolute power from pre-heading to post-heading

We reported the results of the paired t-test for overall change in absolute power in Figure 3.5. As shown in Figure 3.5, there was significant evidence of increases in the absolute power

after heading for all the bands but theta as the p-value of the test was less than the threshold based on the Bonferroni correction for all the bands.

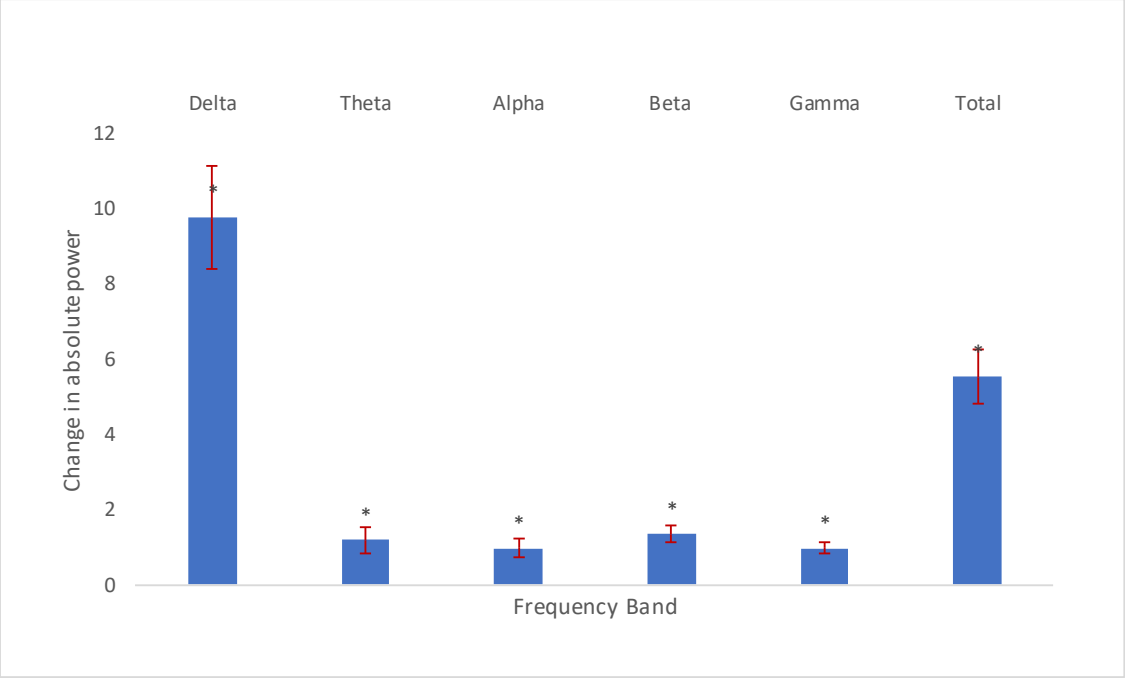

Figure 3.5 Bar graphs of average change in absolute power from pre-heading to post-heading
*Note: ***** stands for the p-value of the paired t-test less than the threshold based on the Bonferroni correction.*

We also examined the association of the change in absolute power due to heading with the two factors of loading direction and impact level and reported the results of the two-way ANOVA in Table 3.1. The change in absolute power is significantly associated with the two factors in all the bands but delta based on the Bonferroni correction threshold. More specifically, the largest change in absolute power was 18.517, 15.106, and 12.619 in theta, beta and gamma bands, respectively, for left loading and impact level of 7 rad/s, and 11.226 and 325.719 in alpha and total bands respectively for right loading and impact level of 7 rad/s. The details of pre- and post-heading statistics with these two factors for absolute power are included in Appendix A.2.

Table 3.1 Regression analysis of absolute power with loading direction and speed

Factor	Frequency Band					
	Delta	Theta	Alpha	Beta	Gamma	Total
Intercept	52.865	-4.902	-2.460	-1.472	2.203	48.599
f1 (left)	79.067	6.754	5.697	*7.216	·5.198	98.829
f1 (right)	·141.021	3.295	·6.005	3.017	-0.119	·152.043
f2 (7 rad/s)	·96.371	*16.665	*7.681	*9.362	*5.418	·125.077
Adjusted R^2	0.010	0.021	0.013	0.030	0.020	0.014
P-value of F-test	·0.0071	*0.0000	*0.0023	*0.0000	*0.0001	*0.0014

Note: ·, stands for the p-value of a test less than 0.05 and the threshold based on the Bonferroni correction respectively.*

In addition, we reported the one-way ANOVA with single factor in Table 3.2. First, the change in absolute power significantly varied for different loading directions only in delta, gamma, and total bands. More specifically, the estimated average change in absolute power was 3.104, 9.864, and 16.316 in delta, 0.594, 1.890, and 1.572 in gamma, and 0.898, 1.716, and 4.124 in total, respectively, for front, left, and right loading directions.

Second, the change in absolute power was significantly different for the two speeds of 4 rad/s and 7 rad/s in all bands except for the delta and total band. Particularly, the estimated average change in absolute power was -0.146 and 2.551 in theta, 0.054 and 1.902 in alpha, 0.303 and 2.394 in gamma, and 0.590 and 1.381 in total, respectively, for the speeds of 4 rad/s and 7 rad/s.

Table 3.2 Regression analysis of absolute power with a single factor

Factor	Frequency Band					
	Delta	Theta	Alpha	Beta	Gamma	Total
	Factor 1 Loading Direction					
Intercept	3.104	0.811	0.344	0.551	0.415	1.957
f1(left)	·6.760	0.471	1.069	·1.500	*1.238	·3.658
f1(right)	*13.213	0.704	0.831	0.893	0.473	*7.034
Adjusted R^2	0.015	-0.001	0.002	0.006	0.015	0.015
P-value of F-test	*0.0003	0.7133	0.1500	·0.0251	*0.0003	*0.0004
	Factor 2 Ball Speed					
Intercept	*7.558	-0.146	0.054	0.303	*0.590	*4.115
f2(7 rad/s)	4.407	*2.697	*1.848	*2.091	*0.791	2.810
Adjusted R^2	0.002	0.015	0.016	0.022	0.009	0.003
P-value of F-test	0.1026	*0.0001	*0.0001	*0.0000	*0.0020	0.0535

Note: ·, stands for the p-value of a test less than 0.05 and the threshold based on the Bonferroni correction respectively.*

Furthermore, we conducted a t-test to examine whether the change due to shams was different from the change due to heading in the frontal direction and displayed the test results in Figure 3.6. There was significant evidence that the change in absolute power for shams differed from the one due to heading with front loading direction and the impact level of 4 rad/s only in alpha and beta bands.

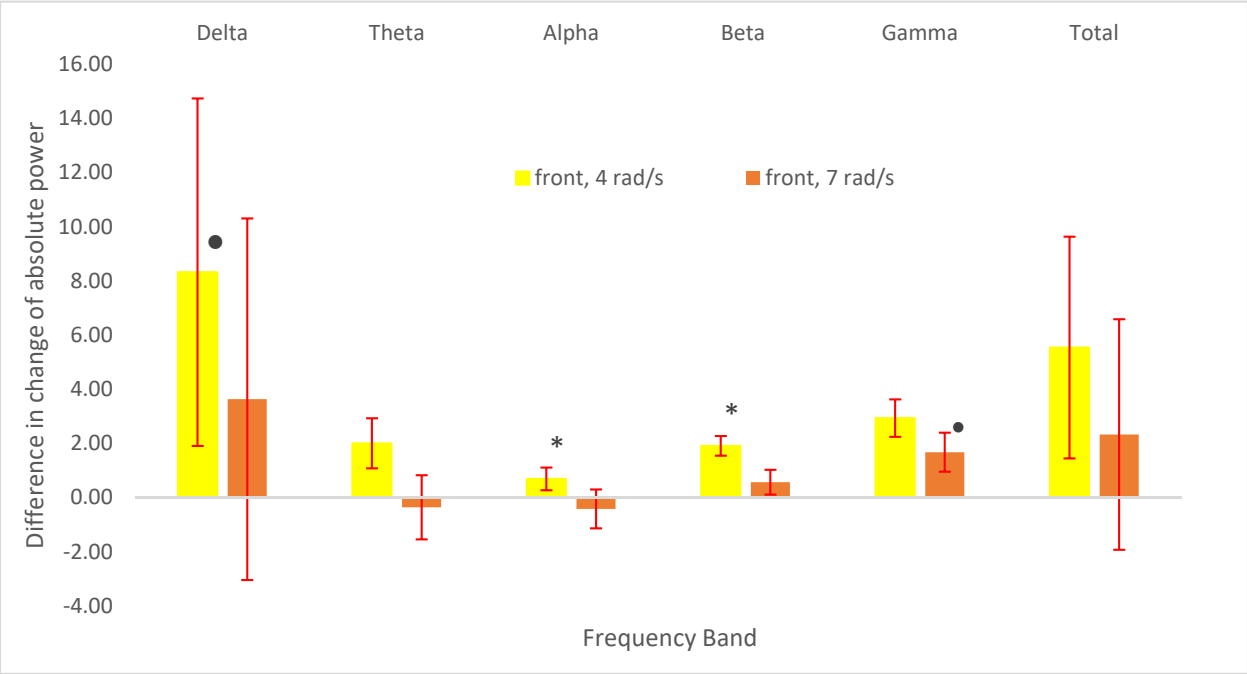

Figure 3.6 The average difference in the change of absolute power between shams and impacts
Note: ●, stand for the p-value of the t-test less than 0.05 and the threshold based on the Bonferroni correction respectively.*

3.4 Relative Power Results

Like absolute power, we measured change in relative power as the difference of the post-heading relative power minus the pre-heading relative power and presented the boxplot of the data in Figure 3.7 with the summary statistics of the data in Appendix B. While the change in relative power was skewed with various degrees for different frequency bands, all the data were in the range from -33.2% to 69.6%, and the average change in relative power is 6.7% for Delta, -2.2% for Theta, -2.7% for Alpha, -1.4% for Beta, and -1.4% for Gamma respectively.

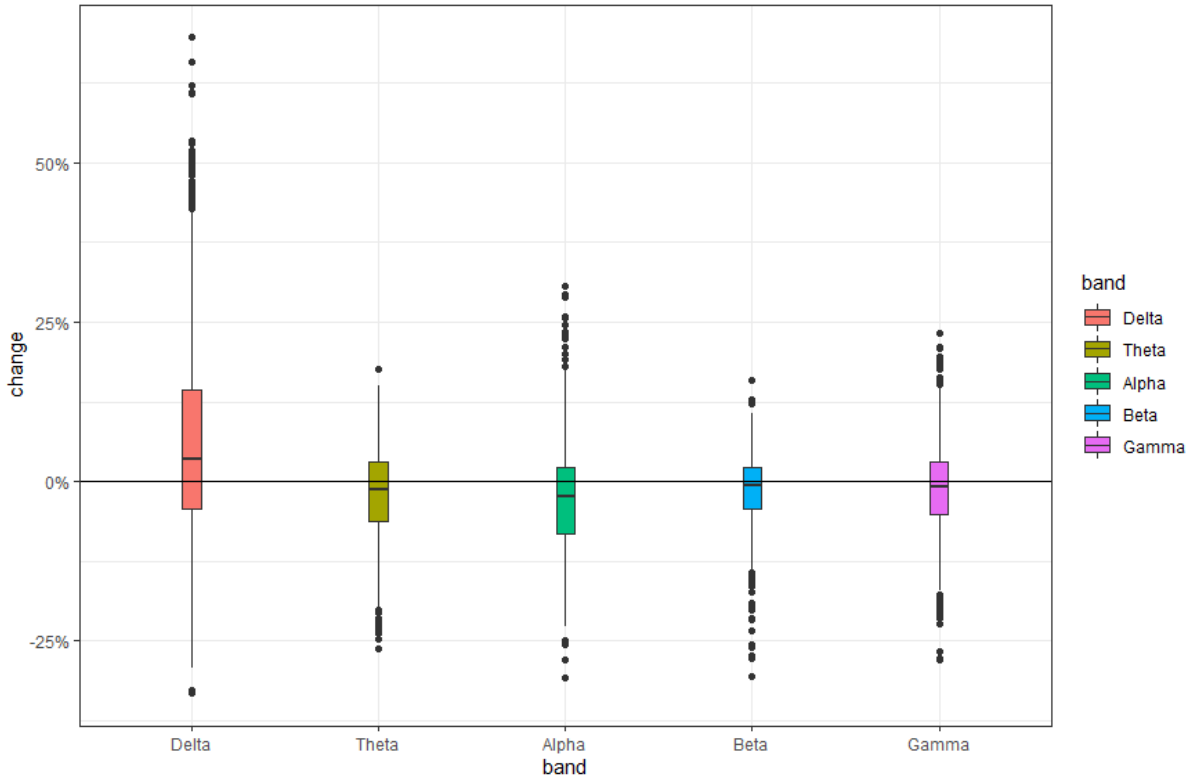

Figure 3.7 Boxplot of change in relative power from pre-heading to post-heading

As in absolute power, we reported the test results for overall change in relative power in Figure 3.8. As shown in Figure 3.8, there was significant evidence that relative power had an increase in delta and a decrease in the other four bands as the p-value of the test was less than the threshold based on the Bonferroni correction for all the bands. Moreover, the effect size of the change in delta was noticeably larger than in other bands.

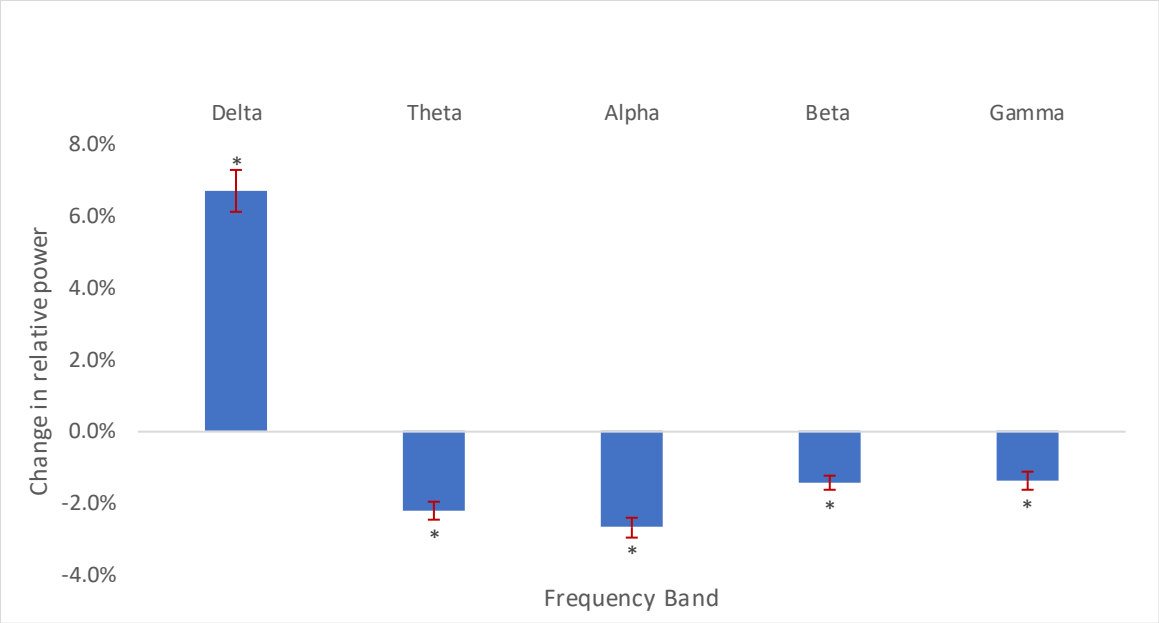

Figure 3.8 The average change in relative power from pre-heading to post-heading.
*Note: * stands for the p-value of the paired t-test less than the threshold based on the Bonferroni correction.*

As in the analysis of absolute power, we reported the results of the two-way ANOVA for relative power in Table 3.3. As showed in the last row in Table 3.3, the change in relative power was significantly associated with the two factors only in theta and gamma. More specifically, the largest (smallest) change in relative power was -0.7% (-3.7%) for front loading and impact level of 7 rad/s (right loading and impact level of 4 rad/s) in theta, and 0.5% (-3.3%) for right loading and impact level of 4 rad/s (front loading and impact level of 7 rad/s) in gamma respectively. The details of pre- and post-heading statistics with the two factors for relative power are in Appendix A.1.

Table 3.3 Regression analysis of relative power with loading direction and speed

Factor	Frequency Band				
	Delta	Theta	Alpha	Beta	Gamma
Intercept	*6.9%	*-2.3%	*-3.1%	*-1.2%	·-1.1%
f1(left)	0.0%	-0.8%	-0.2%	-0.5%	0.7%
f1(right)	-2.4%	·-1.4%	0.8%	0.7%	·1.6%
f2(7 rad/s)	1.2%	*1.6%	0.5%	-0.7%	*-2.2%
Adjusted R^2	0.002	0.014	0.001	0.008	0.025
P-value of F-test	0.1744	*0.0014	0.2976	·0.0181	*0.0000

Note: ·, stands for the p-value of a test less than 0.05 and the threshold based on the Bonferroni correction respectively.*

Additionally, we reported the results of the one-way ANOVA with single factor in Table 3.4. The p-value of F-test was less than the threshold based on the Bonferroni correction only in theta and gamma, there was significant evidence that the change in relative power varied over different impact levels only in theta and gamma. More specifically, the estimated average change in relative power was -3.0% and -1.4% in theta, -0.3% and -2.5% in gamma, for the impact levels of 4 rad/s and 7 rad/s respectively.

Table 3.4 Regression analysis of relative power with a single factor

Factor	Frequency Band				
	Delta	Theta	Alpha	Beta	Gamma
	Factor 1 – Loading direction				
Intercept	*7.5%	*-1.5%	*-2.9%	*-1.5%	*-2.1%
f1(left)	0.0%	-0.8%	-0.2%	-0.5%	0.7%
f1(right)	-2.4%	·-1.4%	0.8%	0.7%	·1.6%
Adjusted R^2	0.002	0.004	0.001	0.006	0.006
P-value of F-test	0.1442	0.0650	0.2559	·0.0305	·0.0291
	Factor 2 – Ball speed				
Intercept	*6.1%	*-3.0%	*-2.9%	*-1.1%	-0.3%
f2(7 rad/s)	1.2%	*1.6%	0.5%	-0.7%	*-2.2%
Adjusted R^2	0.000	0.010	0.000	0.002	0.019
P-value of F-test	0.2966	*0.0015	0.3274	0.0803	*0.0000

Note: ·, stands for the p-value of a test less than 0.05 and the threshold based on the Bonferroni correction respectively.*

We further examined whether the change of relative power for shams was different from the change due to heading with front loading direction and the impact level of either 4 rad/s or 7 rad/s by conducting a t-test for each frequency band and reported the test results in Figure 3.9. Hence, there was significant evidence that the difference in the change of relative power was different between shams and impacts only in theta, beta and gamma for front loading direction and the speed of 4 rad/s and in all the bands but delta for front loading direction and the speed of 7 rad/s respectively. More specifically, the average difference in the change of shams over hit was -4.8% in theta, 2.3% in beta, and 2.9% in gamma for front loading and the speed of 4 rad/s, and -5.6% in theta, -3.1% in alpha, 4.2% in beta, and 7.7% in gamma for front loading and the speed of 7 rad/s respectively. While the sign of the difference in the change between sham and hit were the same in all the frequency bands but delta, the size of the difference is larger for the speed of 7 rad/s than the speed of 4 rad/s.

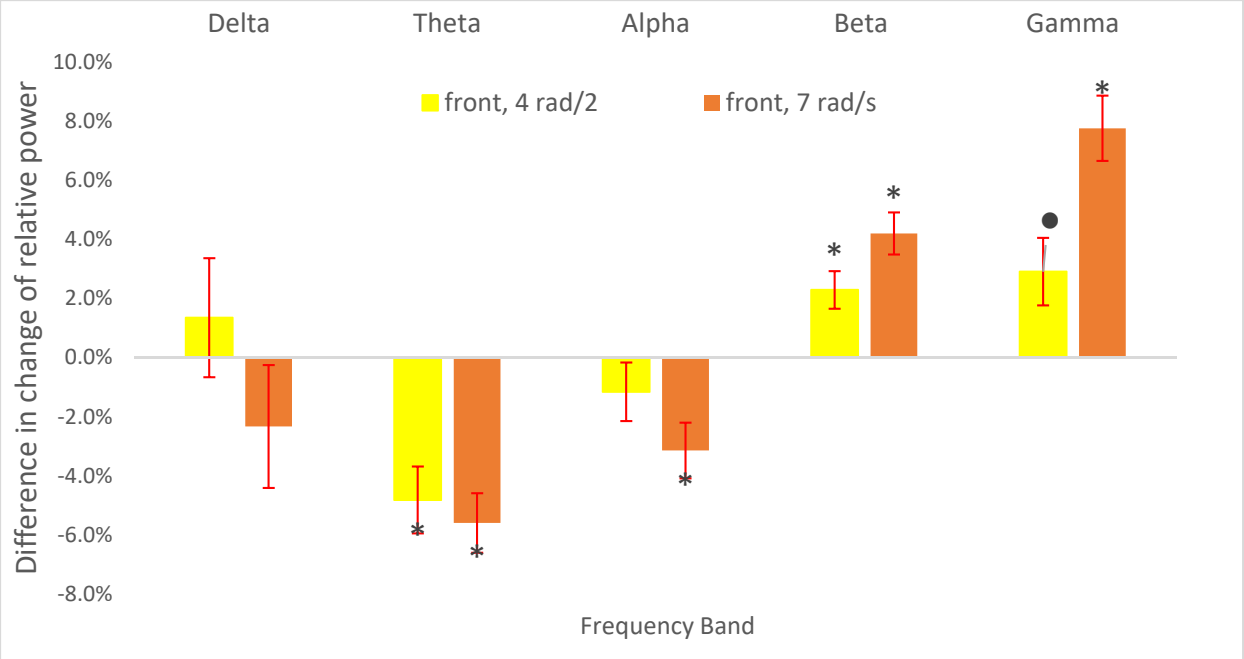

Figure 3.9 The average difference in the change of relative power between shams and impacts
Note: ●, stands for the p-value of a test less than 0.05 and the threshold based on the Bonferroni correction respectively.*

3.5 Discussion

The findings of relative and absolute power from this study showed that we could detect immediate neurophysiological changes due to soccer headers with EEG, and found changes in power in the 2-second period post-heading. More specifically, as EEG power represents amount of activity in certain frequency bands of the EEG signal in the brain (Nunez and Srinivasan, 2005), the immediate neurophysiological change due to heading resulted in an increase in absolute power across all the five frequency bands, suggesting that heading could lead to a surge in amount of activity in the brain. For instance, the increase in power may be due to increased synchronization of the post-synaptic potentials in the brain, which was further evidenced by a higher increase in delta band than in the other bands (Kirschstein, 2009). When there is higher synchronization in the afferents, the amplitudes of the signal will sum together due to constructive interference. An explanation for this increase in power could be due to axonal stretching, which can first result in an increase in extracellular potassium due to damage to the neuron membrane, this would cause depolarization which subsequently leads to neurotransmitter release (Slobounov, 2016). This could contribute to an increase in the number of post-synaptic potentials that the post-synaptic cleft receives in the brain, leading to more summations of these potentials at the pyramidal cells in the brain. Usually axonal stretching would lead to apoptosis in severe cases, however, in these mild cases, it is likely that most of the neurons only had elastic deformations and reverted back to normal.

Furthermore, our findings showed that in terms of absolute power, the immediate neurophysiological change due to heading depended on the two factors considered in the study for all the frequency bands. In particular, the change due to heading was significantly associated with the loading direction (F1) in gamma only, with either left or right loading directions having a larger

increase in absolute power than front loading direction in gamma (see Figure 3.10). The change due to heading was also significantly related to the impact level factor (F2) in alpha, beta and gamma bands with the impact level of 7 rad/s having a larger increase than the impact level of 4 rad/s (see Figure 3.11). This supports the notion that an increase in head impact kinematic as well as side headers could lead to an increase in the neurophysiological change due to headers for soccer players.

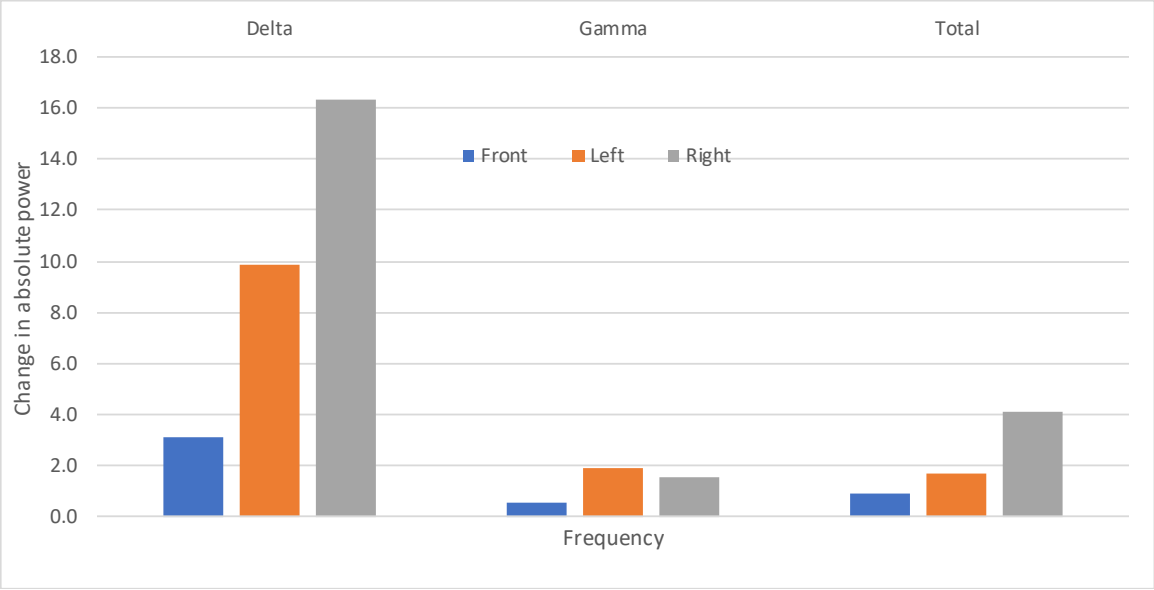

Figure 3.10 The average change in absolute power from pre-heading to post-heading for three loading directions.

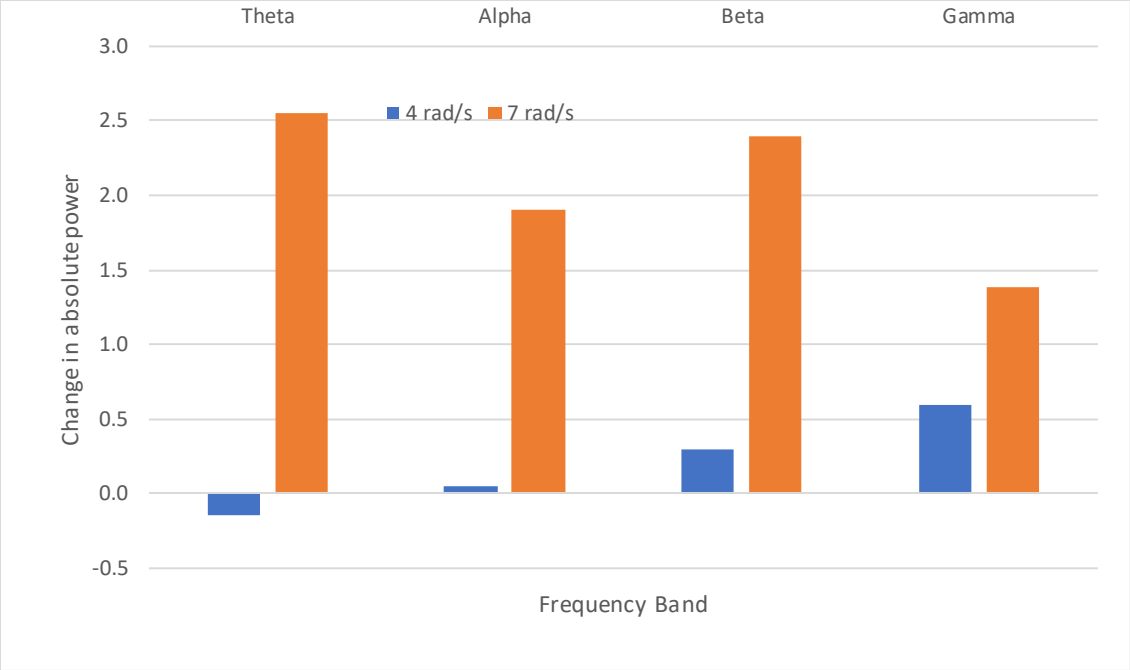

Figure 3.11 The average change in absolute power from pre-heading to post-heading for 4 rad/s and 7 rad/s

Our study found that the immediate neurophysiological change due to heading could also be captured by changes in the relative power post-heading, with a significant increase for delta and a significant decrease for the other four bands, indicating that the proportion of power in delta band dominated in the post-heading EEG signal. It is worth noting that our findings of increases in delta and decreases in alpha were also found in several previous brain injury studies, for example, in a study on post-concussion syndrome (PCS) by Korn et al. (2005), and a study on the breakdown of the blood-brain barrier following TBI by Tomkins et al. (2011). Our study further revealed that in terms of relative power, the change due to heading was related to the two factors only for theta, beta and gamma bands. More specifically, the change due to heading was related to F1 only for beta and gamma with a reduction in relative power for all the three loading directions and more for front and left loading directions than right loading direction (see Figure 3.12). This suggests that the change due to heading may be affected differently by the different directions of the soccer

ball placed on the head. The findings imply that soccer headers could affect player's concentration and attentiveness as several studies in the literature showed that a reduction in beta waves, particularly at the top and front of the scalp, could be an indication of reduced concentration or attentiveness (e.g., Baumeister, 2008 and Buschman et al, 2012).

The change due to heading was associated with F2 only in theta and gamma with a reduction for both frequency band but a larger reduction for the impact level of 4 rad/s in theta and the impact level of 7 rad/s for in gamma (see Figure 3.13). This suggests that an increase in soccer impact level could result in an increase in the ratio of theta over gamma frequency in EEG of soccer players due to heading. Studies have shown that theta-to-gamma relative power spectral density ratio is an important measure for predicting deficits such as working memory function changes, particularly caused by concussions related to sports (e.g., Poltavski et al., 2019).

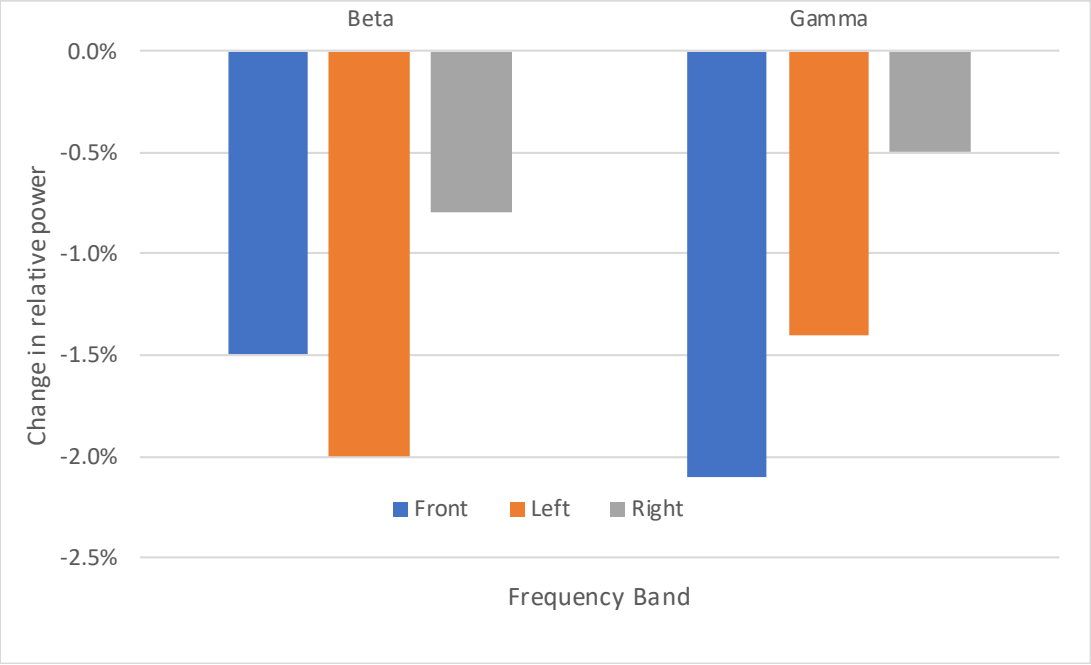

Figure 3.12 The average change in relative power from pre-heading to post-heading for three loading directions.

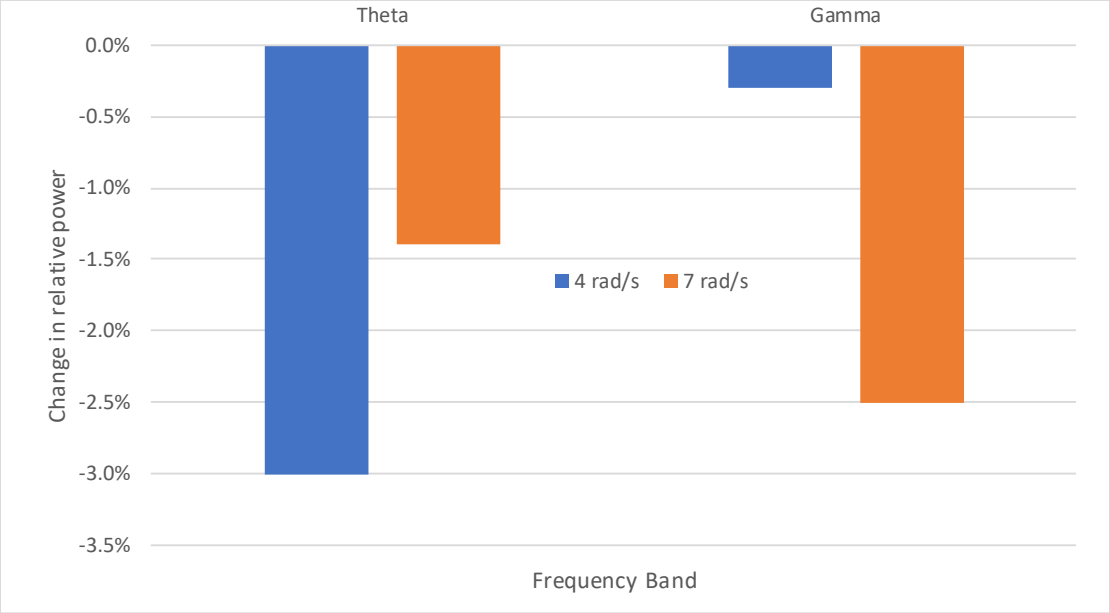

Figure 3.13 The average change in relative power from pre-heading to post-heading for 4 rad/s and 7 rad/s

Finally, our study found that the changes due shams were quite different from those due to heading in some frequency bands with higher differences between the effects of sham headers and actual hits in the 7 rad/s headers than the 4 rad/s headers. This provide further evidence that the changes in power due to heading differentiated from the immediate neurophysiological changes due to the anticipation of heading and that the higher the head kinematics, the more change in the proportions of the frequency bands.

As demonstrated in Newson and Tiagarajan (2019), it is worth noting that characteristic patterns of power change within specific frequency bands may have different interpretations in terms of brain impairments and are not necessarily unique to any one impairment but show substantial overlap across impairments as well as variability within impairment. As such, one should take caution when interpreting changes in specific frequency bands and linking it to one neurologic or neurophysiological deficit in isolation.

Chapter 4: Post-Impact Changes in EEG Coherence

4.1 Functional Connectivity through Coherence Analysis

In this study, we carried out coherence analysis with two measures of coherence with EEG data, namely magnitude squared coherence and imaginary coherence, for the analysis of controlled headers on brain's functional connectivity. Specifically, we considered the changes in magnitude squared coherence and imaginary coherence from pre-heading to post-heading and examined whether and how the immediate neurophysiological changes due to heading were associated with brain's functional connectivity.

As there are 19 electrodes used in our study, the total number of possible pairs of electrodes is 171. However, in our study, we followed the two-compartmental model of EEG coherence proposed by Thatcher et al. (1986) and considered only the coherences of the well-established pairs related to cortico-cortical associations for the analysis of the brain's functional connectivity. By analyzing coherence for these pairs, we were able to evaluate whether the changes in coherence were mostly related to the impairment of short axonal fibers or long axonal fibers and specific electrodes. More specifically, as in Locatelli et al. (1998), we classified the coherence pairs considered in our study into eight groups, namely, 1. local anterior, 2. local posterior, 3. far coherence, 4. prefrontal to frontal and central, 5. occipital to parietal and central, 6. prefrontal to parietal, 7. frontal to occipital, and 8. prefrontal to occipital, with each group including pairs of electrodes as listed in Table 4.1 and visualized in Figure 4.1. Note that groups 1, 2, 4, and 5 are related to the short axonal fibers, and groups 3, 6, 7, and 8 to long axonal fibers. Note also that this classification was applied to both magnitude-squared coherence and imaginary coherence in our study.

Table 4.1 Classification of 19 electrodes according to their locations on a scalp map

Coherence group	Pairs of electrodes
1. local anterior	Fp1-F7, Fp2-F8, F7-C3, F4-C4, C4-F8
2. local posterior	T5-C3, T5-O1, C3-P3, C4-P4, C4-T6, T6-O2
3. far coherence	Fp1-T5, Fp2-T6, F7-T5, F7-P3, F7-O1, T5-F3, F3-P3, F4-P4, P4-F8, F8-T6, F8-O2
4. prefrontal to frontal and central	Fp1-F3, Fp1-C3, Fp2-F4, Fp2-C4
5. occipital to parietal and central	C3-O1, P3-O1, C4-O2, P4-O4
6. prefrontal to parietal	Fp1-F3, Fp1-C3, Fp2-F4, Fp2-C4
7. frontal to occipital	F3-O1, P4-O2
8. prefrontal to occipital	Fp1-O1, Fp2-O2

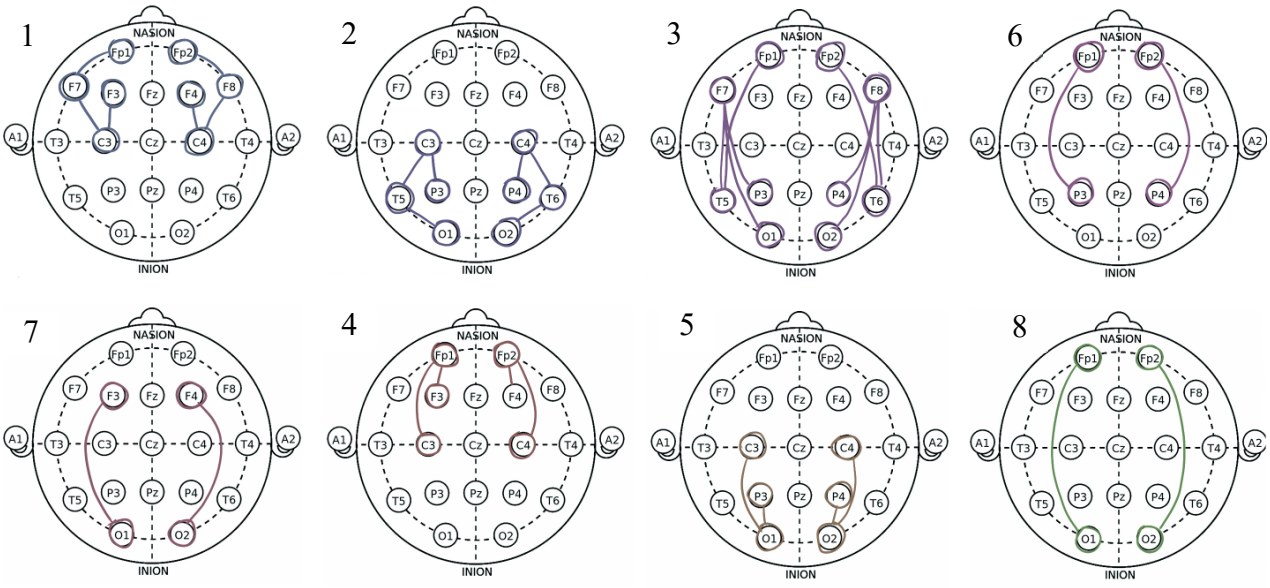

Figure 4.1 Classification of coherence groups on the scalp map

In the analysis of coherence data, for the effects of soccer headers on brain connectivity for each participant, we computed the two coherence measures of each pair of two electrodes and displayed the coherences at each electrode in a scalp map in which each circle shows the location of an electrode and the coherences of this electrode with the other 18 electrodes. For example, Figure 4.2 is such scalp map for magnitude squared coherence in alpha band for a participant in our experiment. Each small circle in Figure 4.2 represents the location of an electrode on the scalp of this participant and the color of the circle for the change in the magnitude squared coherence of

the electrode with the other 18 electrodes from pre-heading to post-heading in alpha band. Particularly, according to the color of circles as shown in Figure 4.2, for this participant, the magnitude squared coherences with other electrodes increased for electrodes O1 and O2 and decreased for electrode Fp1.

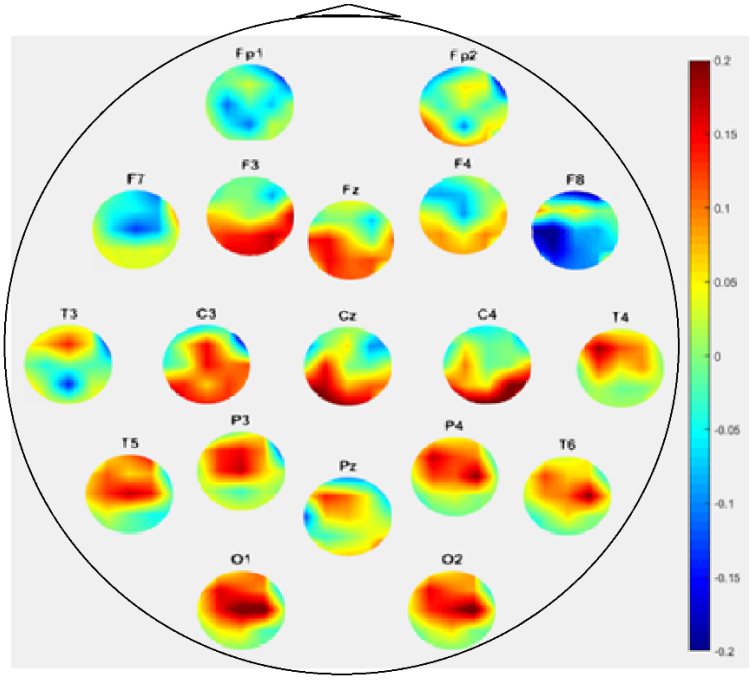

Figure 4.2 Change in magnitude squared coherence from pre-heading to post-heading in alpha band for one participant for a 4 rad/s frontal impact

4.2 Statistical Analysis of Coherence Data

With the use of the same processed EEG data as in for the power analysis in Chapter 3, we employed the same statistical method for coherence data. Particularly, we first conducted a paired t-test for each band to determine whether the overall change in either magnitude squared coherence or imaginary coherence due heading was significant. Furthermore, we conducted three-way ANOVA with loading direction (F1), impact level (F2), and electrode group (F3) to analyze the

association of the change in either of the two coherence measures with the three factors, which can be expressed by the regression of the change in coherence (y_i) on the three factors as follows:

$$y_i = \beta_0 + \beta_1 F_{1,i} + \beta_2 F_{2,i} + \beta_3 F_{3,i} + \varepsilon_i . \quad (5)$$

Note that F1 and F2 are the same as in the analysis of power data and F3 has eight different levels for the coherence groups defined in Table 4.1. Moreover, we conducted one-way ANOVA with single factor to examine the association of the change in each of the two coherence measures with different levels of the factor. The statistical tests performed here has been summarized in Chapter 2.5.

Note that for the statistical analysis of coherence data, we also addressed the issue of possible inflated Type I error in multiple analyses on the same data by performing the Bonferroni correction. The threshold based on the Bonferroni correction with 32 tests for coherence data was 0.0016, which controls the overall probability of Type I error for all the statistical inferences within 0.05.

4.3 Magnitude Squared Coherence Results

As in the analysis of relative and absolute power, we analyzed the change in brain's functional connectivity between the post-heading and pre-heading in terms of the two coherence measures: magnitude squared coherence and imaginary coherence. For the data of magnitude squared coherence from our experiment, we calculated the difference in coherence between post-heading and pre-heading and displayed the boxplot of the data in Figure 4.3 with the summary statistics given in Appendix B. As shown in Figures 4.3, the changes in magnitude squared coherence are mostly symmetrically distributed and centred around zero change, except theta, whose mean change showed a slight decrease.

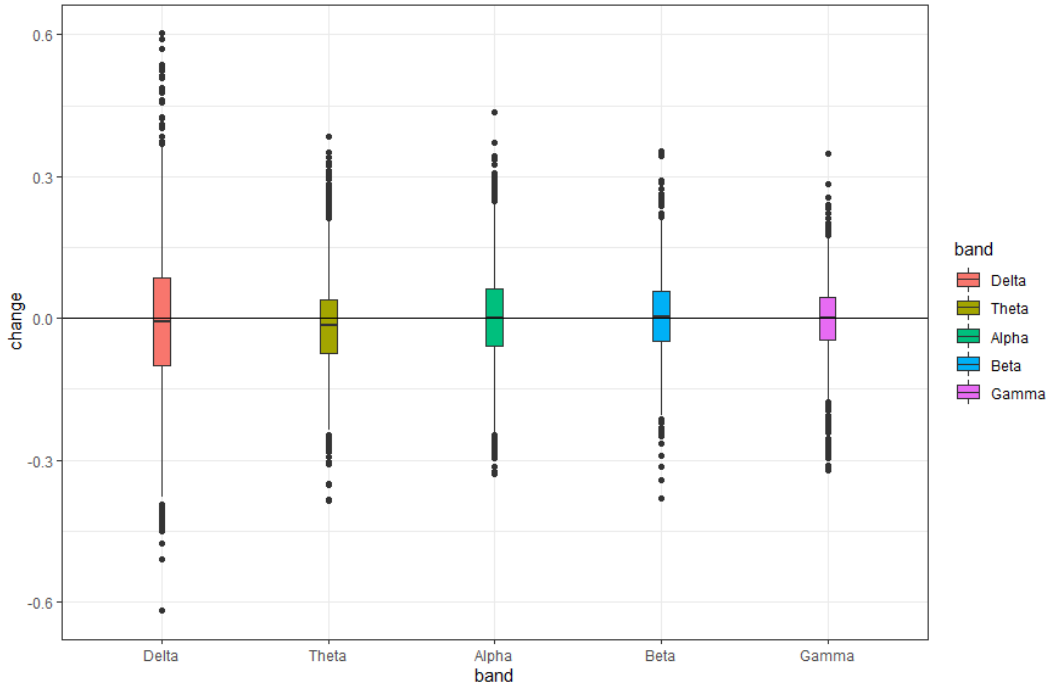

Figure 4.3 Boxplot of change in magnitude squared coherence from pre-heading to post-heading

We reported the results of the paired t-test for overall change in coherence in Figure 4.4. As displayed in Figure 4.4, there was significant evidence that the overall coherence on average decreased after heading for theta.

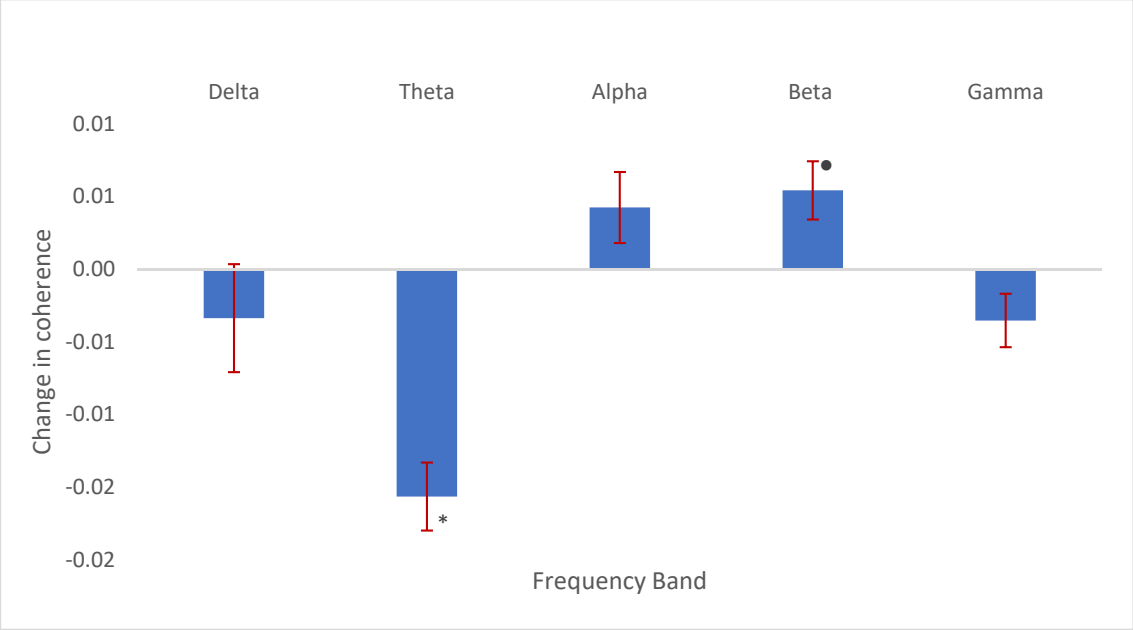

Figure 4.4 The average change in magnitude squared coherence from pre-heading to post-heading.
Note: ●, stands for the p-value of a test less than 0.05 and the threshold based on the Bonferroni correction respectively.*

The three-way ANOVA results for coherence are shown in Table 4.3. As the p-value of the F-test was less than the threshold based on the Bonferroni correction in all the five frequency bands, there was significant evidence that the change in magnitude squared coherence due to heading was associated with the three factors in all the bands. More specifically, the theta band had a larger effect size in both side headers but a smaller effect size in the 7 rad/s header. The right headers also had a larger effect size in the delta and alpha bands. Electrode group 3 had a smaller effect size in the delta band compared to the others. The details of pre- and post-heading statistics with the three factors for magnitude squared coherence are in Appendix A.3.

Table 4.2 Regression analysis of magnitude squared coherence with loading direction, speed and electrode group

Factor	Frequency Band				
	Delta	Theta	Alpha	Beta	Gamma
Intercept	-0.003	-0.011	·0.023	0.003	0.000
f1(left)	·-0.023	*-0.026	·-0.017	0.002	·-0.012
f1(right)	*-0.028	*-0.029	*-0.029	0.002	·0.010
f2(7 rad/s)	-0.002	*0.023	-0.007	-0.002	-0.004
f3(2)	0.012	-0.007	-0.014	-0.008	-0.009
f3(3)	*0.040	·0.019	0.014	0.011	0.001
f3(4)	-0.010	·-0.024	·-0.022	·-0.017	-0.006
f3(5)	0.005	-0.009	-0.005	0.011	0.004
f3(6)	0.014	-0.007	-0.017	·-0.020	-0.005
f3(7)	0.028	0.019	·0.028	·0.022	0.005
f3(8)	0.018	0.002	-0.002	-0.001	0.008
Adjusted R^2	0.014	0.047	0.028	0.014	0.012
P-value of F-test	*0.0002	*0.0000	*0.0000	*0.0002	*0.0005

Note: ·, stands for the p-value of a test less than 0.05 and the threshold based on the Bonferroni correction respectively.*

Furthermore, we reported the results of the one-way ANOVA with single factor for magnitude squared coherence in Table 4.3. Specifically, first, the changes due to loading direction

in the theta, alpha and gamma band were significant. Particularly, among theta, alpha and gamma bands, the largest increase occurred for front loading in alpha, and the largest decrease occurred for right loading in theta respectively (see Figure 4.5).

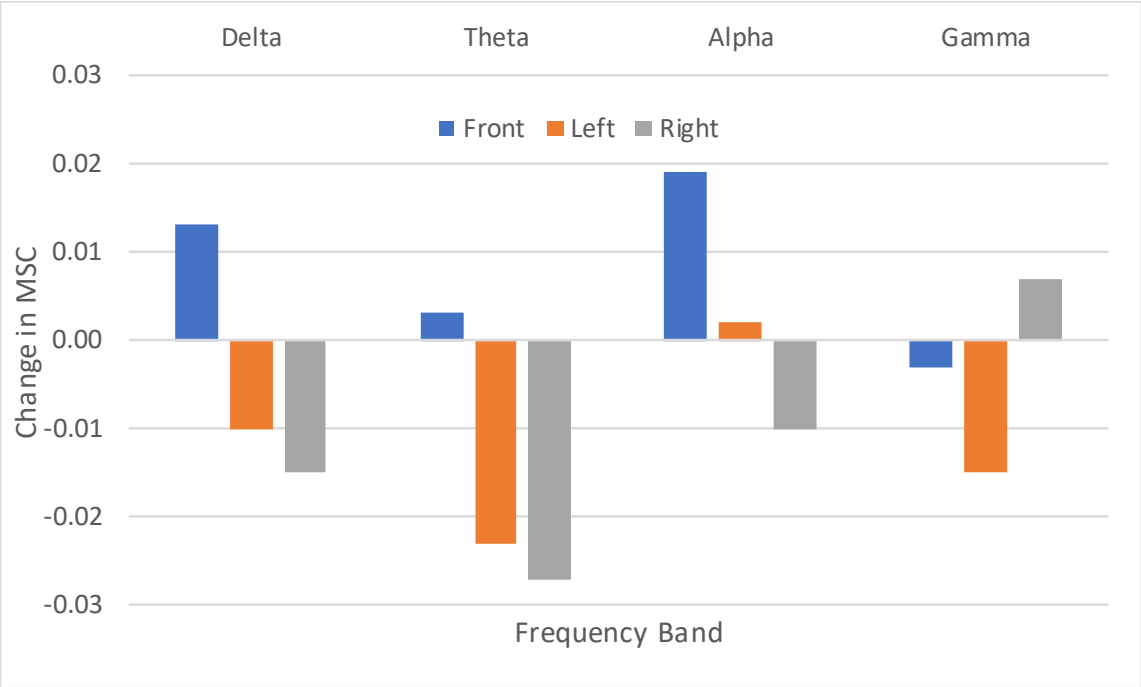

Figure 4.5 The average change in magnitude squared coherence from pre-heading to post-heading for three loading directions.

The change in magnitude squared coherence significantly differed for the impact levels of 4 rad/s and 7 rad/s only in theta. The estimated average change in magnitude squared coherence for theta band was -0.027 for the impact level of 4 rad/s and -0.004 for the impact level of 7 rad/s respectively. The changes due to electrode groups were significant in the theta, alpha and beta bands.

Table 4.3 Regression analysis of magnitude squared coherence with a single factor

Factor	Frequency Band				
	Delta	Theta	Alpha	Beta	Gamma
	Factor 1 – Loading direction				
Intercept	·0.013	0.003	*0.019	0.004	-0.003
f1(left)	·-0.023	*-0.026	·-0.017	0.002	·-0.012
f1(right)	·-0.028	*-0.030	*-0.029	0.002	·0.010
Adjusted R^2	0.005	0.017	0.012	-0.001	0.012
P-value of F-test	·0.0043	*0.0000	*0.0000	0.8834	*0.0000
	Factor 2 – Ball speed				
Intercept	-0.003	*-0.027	·0.007	·0.006	-0.001
f2(hard)	-0.001	*0.023	-0.006	-0.002	-0.005
Adjusted R^2	-0.001	0.013	0.000	0.000	0.000
P-value of F-test	0.8615	*0.0000	0.2171	0.6317	0.2133
	Factor 3 – Electrode group				
Intercept	·-0.021	·-0.018	0.005	0.004	-0.003
f3(2)	0.012	-0.007	-0.014	-0.008	-0.009
f3(3)	*0.040	·0.019	0.014	0.011	0.001
f3(4)	-0.010	·-0.024	·-0.022	·-0.017	-0.006
f3(5)	0.005	-0.009	-0.005	0.011	0.004
f3(6)	0.014	-0.007	-0.017	·-0.020	-0.005
f3(7)	0.028	0.019	·0.028	·0.022	0.005
f3(8)	0.018	0.002	-0.002	-0.001	0.008
Adjusted R^2	0.009	0.017	0.015	0.015	0.000
P-value of F-test	·0.0016	*0.0000	*0.0000	*0.0000	0.3998

Note: ·, stands for the p-value of a test less than 0.05 and the threshold based on the Bonferroni correction respectively.*

We also investigated whether the change in magnitude squared coherence due to shams was different from the change due to heading with front loading direction and either 4 rad/s or 7 rad/s and reported the test results in Figure 4.6. There was significant evidence that the difference in the change of magnitude squared coherence was different between shams and impacts in the front loading direction and the impact level of 4 rad/s in all the frequency bands but delta and the front loading direction and the impact level of 7 rad/s only in delta and theta respectively.

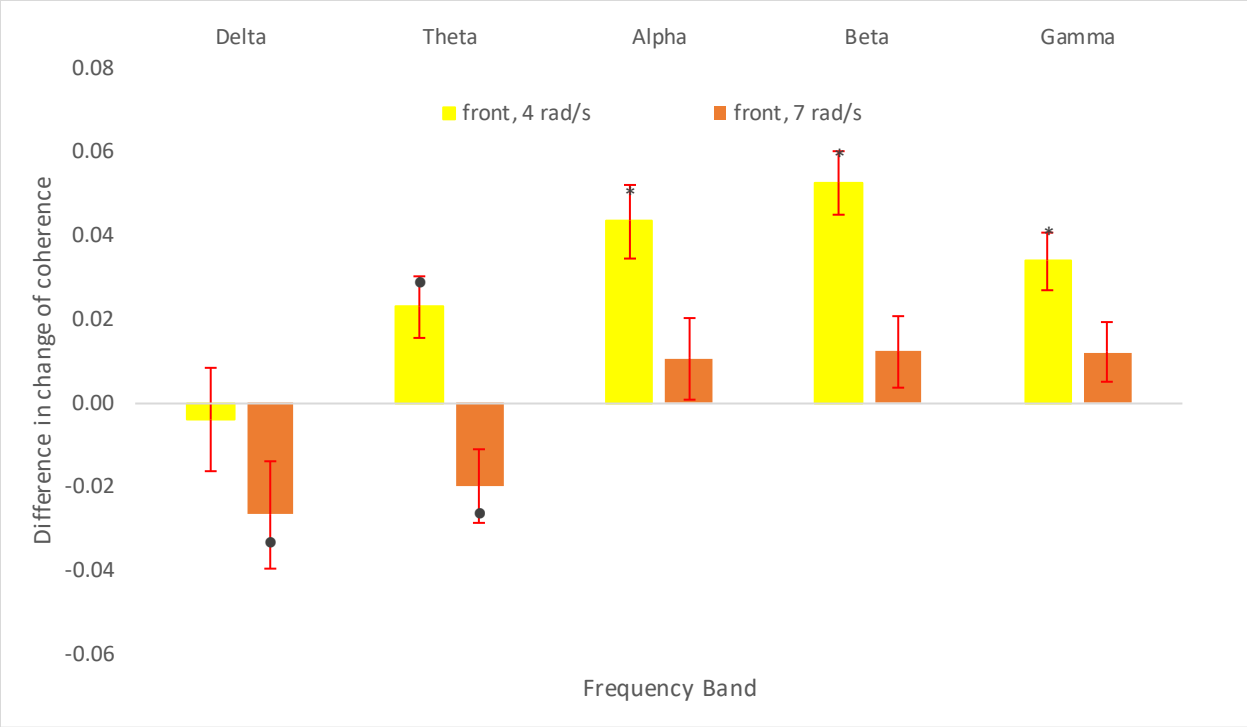

Figure 4.6 The average difference in the change of magnitude squared coherence between shams and impacts.
*Note: ●, * stand for the p-value of a test less than 0.05 and the threshold based on the Bonferroni correction respectively.*

4.4 Imaginary Coherence Results

For the data of the change in imaginary coherence, we presented its boxplots Figures 4.7 with its summary statistics given in Appendix B. As shown in figure 4.7, the change in imaginary coherence is mostly symmetrically distribution and centred around 0 change for each frequency band.

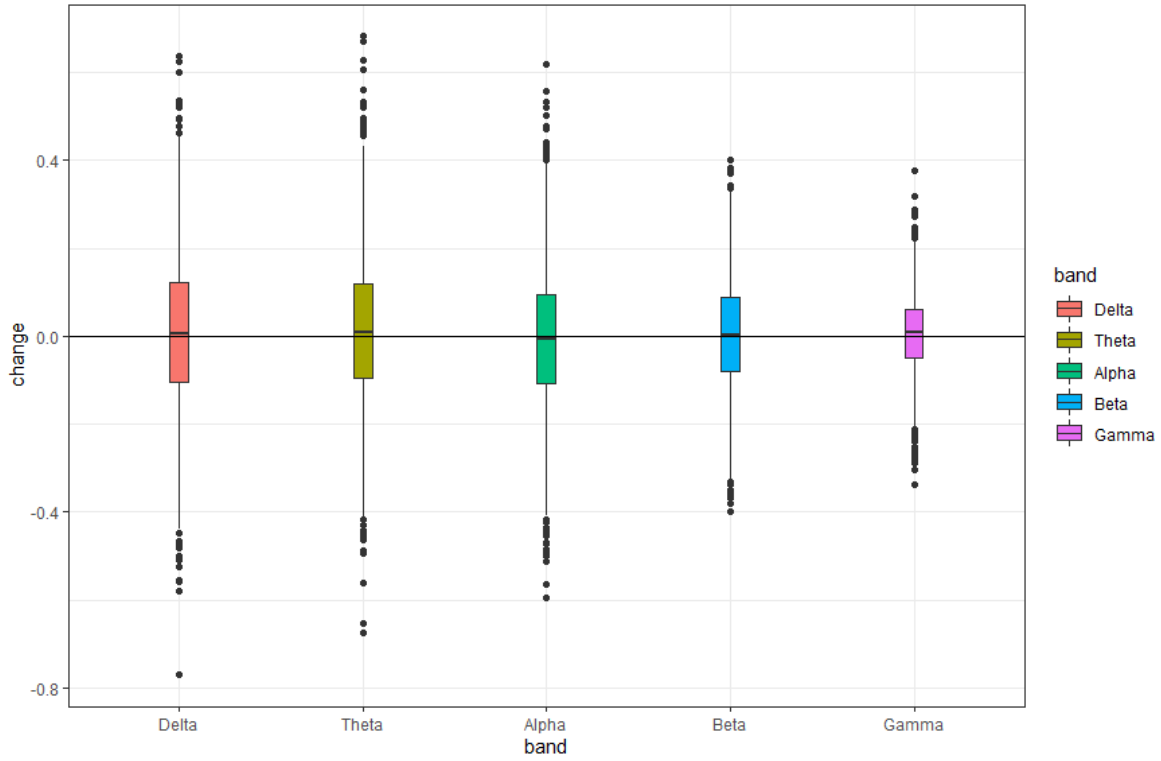

Figure 4.7 Boxplot of change in imaginary coherence from pre-heading to post-heading

We reported the results of the paired t-test for overall change in imaginary coherence in Figure 4.8. There were no significant differences between the pre-impact and post-impact imaginary coherence.

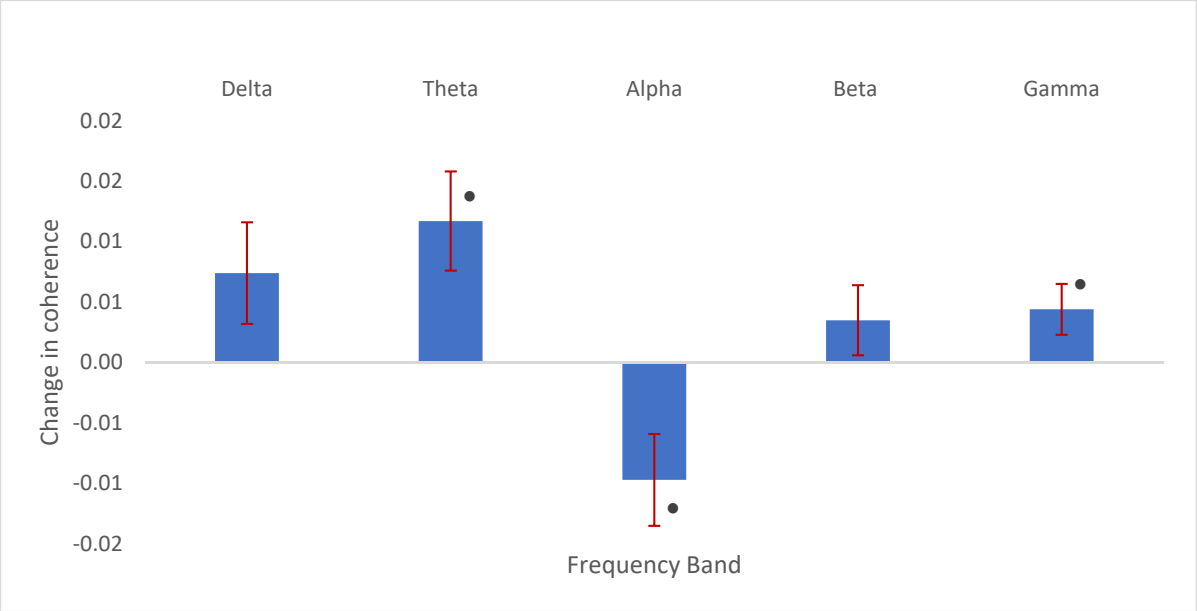

Figure 4.8 The average change in imaginary coherence between pre-heading and post-heading.
Note: ● stands for the p-value of the t-test less than 0.05.

Like magnitude squared coherence, we reported the results of the three-way ANOVA for imaginary coherence in Table 4.4. There were no significant changes in the imaginary coherence in any of the 3 factors. The details of pre- and post-heading statistics with the three factors for imaginary coherence are in Appendix A.4.

Table 4.4 Regression analysis of imaginary coherence with loading direction, ball speed, and electrode group

Factor	Frequency Band				
	Delta	Theta	Alpha	Beta	Gamma
Intercept	-0.008	0.004	0.010	-0.010	0.000
f1(left)	·0.022	0.009	0.007	0.007	-0.003
f1(right)	·0.025	0.006	-0.005	0.007	0.007
f2(hard)	0.011	-0.003	-0.008	·0.015	-0.003
f3(2)	-0.014	0.002	-0.012	-0.001	-0.001
f3(3)	-0.003	0.000	·-0.030	-0.010	0.011
f3(4)	-0.002	-0.009	-0.006	0.020	0.014
f3(5)	-0.008	0.024	-0.014	0.004	-0.008
f3(6)	-0.010	-0.011	0.003	0.017	0.015
f3(7)	0.000	·0.047	-0.027	0.001	-0.018
f3(8)	-0.008	0.013	-0.021	0.017	·0.023
Adjusted R^2	0.000	0.001	0.002	0.006	0.009
P-value of F-test	0.4575	0.2894	0.2205	·0.0266	·0.0043

Note: · stands for the p-value of a test less than 0.05.

We also reported the results of the one-way ANOVA for imaginary coherence in Table 4.5. Again, there were no significant changes among the individual factors.

Table 4.5 Regression analysis of imaginary coherence with a single factor

Factor	Frequency Band				
	Delta	Theta	Alpha	Beta	Gamma
	Factor 1 – Loading direction				
Intercept	-0.008	0.007	-0.011	-0.001	0.003
f1(left)	·0.022	0.009	0.007	0.007	-0.003
f1(right)	·0.025	0.006	-0.005	0.007	0.007
Adjusted R^2	0.003	-0.001	0.000	0.000	0.001
P-value of F-test	·0.0319	0.6397	0.4656	0.5133	0.1738
	Factor 2 – Ball speed				
Intercept	0.002	·0.013	-0.006	-0.004	·0.006
f2(hard)	0.011	-0.003	-0.008	·0.015	-0.003
Adjusted R^2	0.000	-0.001	0.000	0.003	0.000
P-value of F-test	0.2130	0.6908	0.2744	·0.0091	0.4709
	Factor 3 – Electrode group				
Intercept	0.013	0.007	0.006	0.002	-0.001
f3(2)	-0.014	0.002	-0.012	-0.001	-0.001
f3(3)	-0.003	0.000	·-0.030	-0.010	0.011
f3(4)	-0.002	-0.009	-0.006	0.020	0.014
f3(5)	-0.008	0.024	-0.014	0.004	-0.008
f3(6)	-0.010	-0.011	0.003	0.017	0.015
f3(7)	0.000	·0.047	-0.027	0.001	-0.018
f3(8)	-0.008	0.013	-0.021	0.017	·0.023
Adjusted R^2	-0.003	0.002	0.002	0.003	0.008
P-value of F-test	0.9897	0.1434	0.1742	0.0999	·0.0029

Note: · stands for the p-value of a test less than 0.05.

Similarly, we also investigated whether the change in imaginary coherence due to shams was different from the change due to heading with front loading direction and either 4 rad/s or 7 rad/s by conducting a t-test for each frequency band and reported the test results in Figure 4.9. There was significant evidence that the difference in the change of imaginary coherence was different between shams and impacts in the front loading direction and the impact level of 4 rad/s only in alpha and gamma, and the front loading direction and the impact level of 7 rad/s in the theta and

alpha bands respectively. The sign of the difference was the same for the two speeds in all the bands.

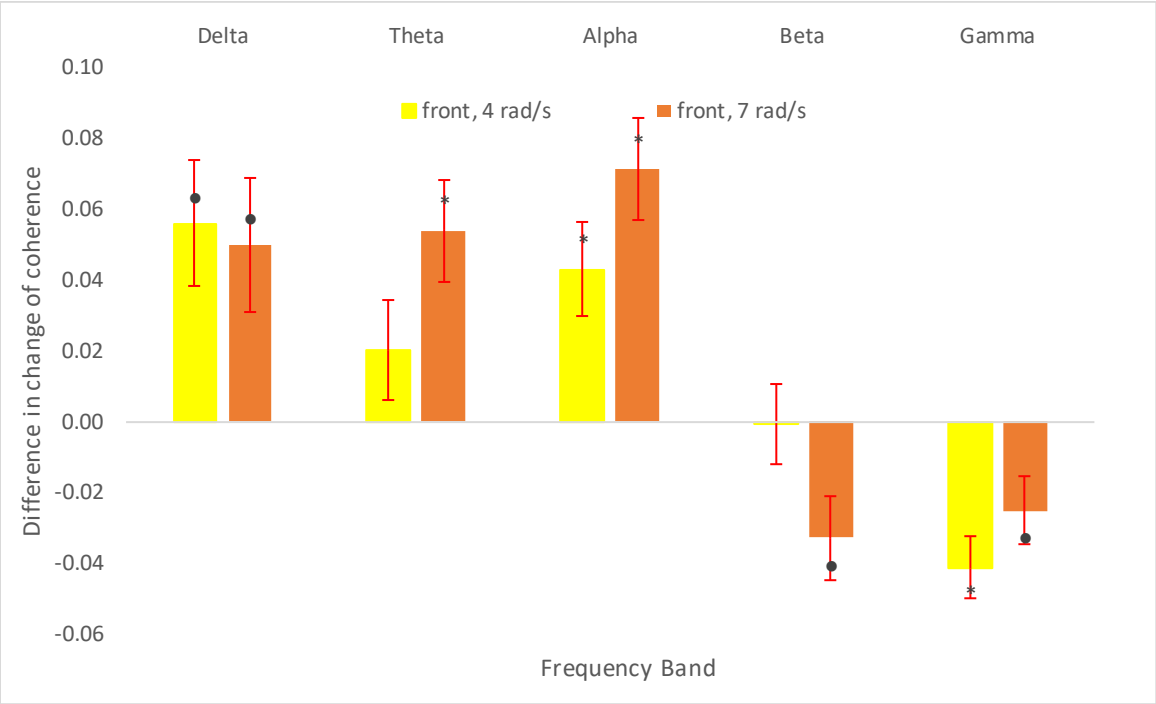

Figure 4.9 The average difference in the change of imaginary coherence between shams and impacts
Note: ●, stand for the p-value of a test less than 0.05 and the threshold based on the Bonferroni correction respectively.*

4.5 Discussion

In addition to the power changes, we also found statistically significant coherence changes in EEG in the 2-second period post-heading. More specifically, our study found that the immediate neurophysiological change due to heading could be measured by overall change in magnitude squared coherence from pre-heading to post-heading with a significant decrease in theta and a significant increase in beta respectively. As change in coherence between two electrodes on scalp could be interpreted as change in interaction of the underlying neuronal regions, the findings

suggest that soccer headers may affect overall interaction between the underlying neuronal regions with a decrease in theta and an increase in beta respectively. Decreases in the theta coherence was also observed in patients with Alzheimer Disease according to a study (Besthorn, 1994). Besthorn interpreted the decrease in the theta coherence as widespread cerebral degenerations as it pertains to Alzheimer Disease, this would then lead to fewer neuronal connections. Perhaps a much milder and temporary version of decreased connectivity may have occurred upon receiving the head impact.

More importantly, in terms of magnitude squared coherence, the change due to heading was significantly associated with the three factors for all the five frequency bands. As shown in Figure 4.5, it suggested that different loading directions could have different effects on brain's functional connectivity. The change due to heading was significantly related to F3 in all the bands except gamma, with alpha band having much larger increases in magnitude squared coherence than the other three bands for all the coherence groups, particularly the frontal to occipital coherence group (see Figure 4.11). The results show that for all the bands except beta, the largest increases in coherence occurred in the long axonal groups and the decreases in coherence occurred in the anterior short axonal fibers. This suggests the need for further investigating whether soccer headers may reduce brain's functional connectivity particularly at the anterior part of the scalp that hit by the ball in our experiment.

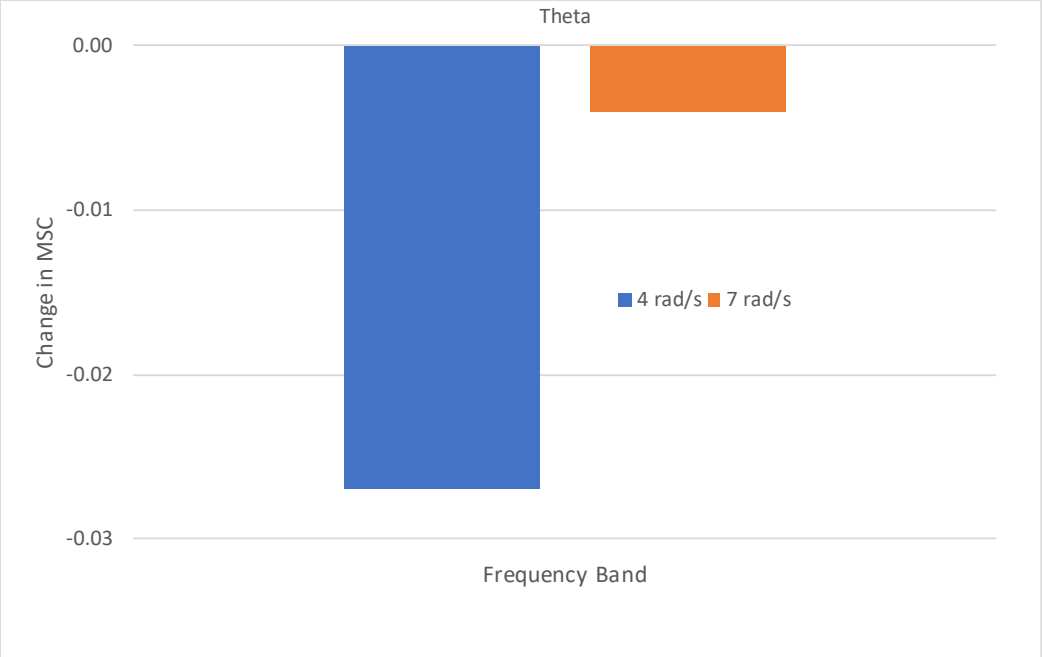

Figure 4.10 The average change in magnitude squared coherence from pre-heading to post-heading for 4 rad/s and 7 rad/s.

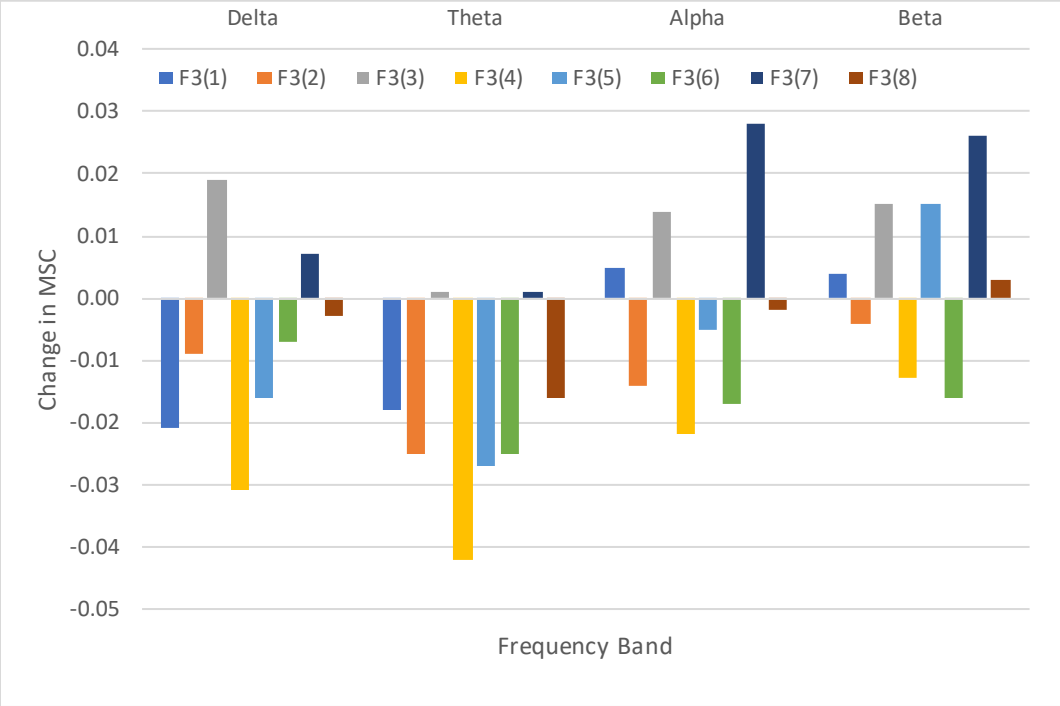

Figure 4.11 The average change in magnitude squared coherence from pre-heading to post-heading for eight coherence groups.

Our study found no significant evidence of immediate neurophysiological changes in the imaginary coherence due to heading . This contrasts with the findings in the magnitude-squared coherence in terms of the functional connectivity. This discrepancy could be due to imaginary coherence measures ignoring a portion of interaction in the real component, which could lead to less reliable localizations of interactions compared to the magnitude-squared coherence (Guggisberg, 2011). Moreover, there is also evidence that if the real component is relatively much large, imaginary coherence can fail to detect even strong interactions (Bornot, 2018).

Finally, our study found that the changes in coherence due to shams were significantly different from those due to heading for most of the frequency bands. This provide further evidence that the changes in coherence due to heading differentiated from the immediate neurophysiological changes due to the anticipation of heading.

Chapter 5: EEG Recovery and Neuropsychological Evaluation

Subconcussive head impacts are largely unexamined and are not expected to lead to observable symptoms (Bailes et al. ,2013, Talavage, 2013). This lack of observable symptoms for sub-concussive impacts may be due to a quick recovery in the neurophysiological changes after these impacts. Hence, in this study, we were interested in evaluating how quickly the immediate neurophysiological changes due to heading could recover after each header by analyzing the EEG changes over different post-impact epoch lengths. Additionally, we examined whether multiple headers performed in succession could have any cumulative and lasting changes. As such, we focused on the effects of receiving multiple headers in terms of neurophysiological changes and cognitive changes.

5.1 Post Impact Recovery

To evaluate whether the participants recover from these simulated headers, we first examined whether immediate neurophysiological changes due to heading during the trials diminished over time. For this purpose, we compared the changes in the absolute and relative power over the 2-second and 5-second post-impact epochs. Figure 5.1 displays the average change in absolute power using the 2-second epochs (orange bar) and 5-second epochs (blue bar) respectively together with the difference of the 5-second epoch change over the 2-second epoch change (grey bar). As shown in Figure 5.1, while absolute power increased after heading for both the 2-second and 5-second epochs in each frequency band, the size of increase was less when using the 5-second epoch than the 2-second epoch in each frequency band. In addition, we showed that change in absolute power in the 5-second epoch was significantly less than the 2-second epoch across all the bands based on a t-test. This result suggests that the participants could recover from the controlled headers quickly as the effects of the header diminished over time.

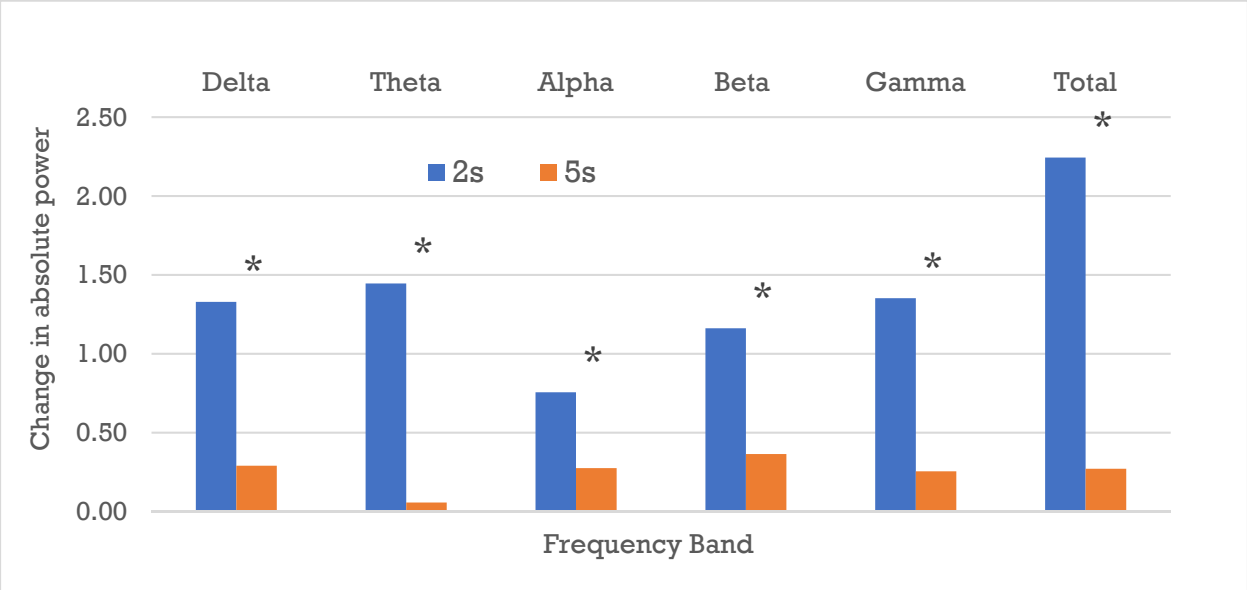

Figure 5.1 The average change in absolute power from pre-heading to post-heading for 2-second and 5-second epochs.
*Note: * stands for the p-value of the t-test less than 0.05.*

Similarly, Figure 5.2 displays the average change in relative power from pre-heading to post-heading for 2-second epoch (orange bar) and 5-second epoch (blue bar) respectively together with the difference of the 5-second epoch over the 2-second epoch (grey bar). Clearly, the sign of the change in relative power was the same for both the 2-second and 5-second epochs in each frequency band, but the size of the change differed. Moreover, we showed that the change for the 5-second epoch was significantly less than that for the 2-second epoch for the relative power with the use of a t-test; this provided evidence that the effects of the header diminished over time. Hence, the findings based on both absolute and relative power show that the recovery from controlled headers of the participants in our experiment was quick with no significant evidence of adverse consequences for the participants due to the experiment.

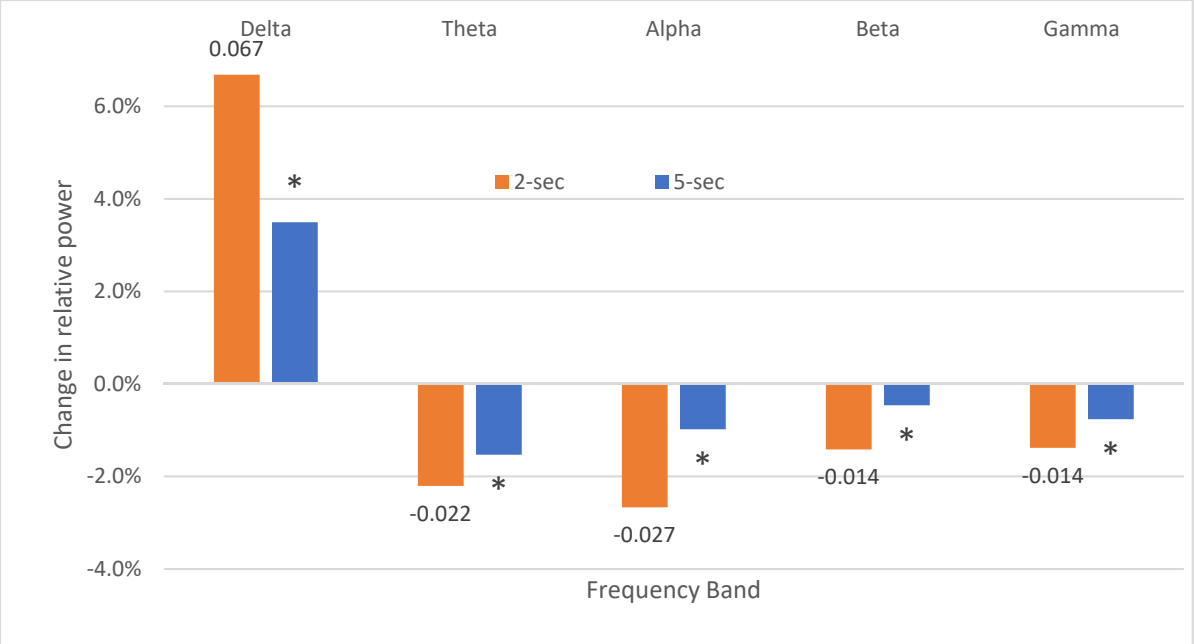

Figure 5.2 The average change in relative power from pre-heading to post-heading for 2-second and 5-second epochs.
Note: ● stands for the p-value of the t-test less than 0.05.

5.2 Post Session Recovery

For this study, we have also investigated whether there is any evidence of neurocognitive changes after all of the controlled head impacts. For this purpose, we conducted a neurocognitive test for each participant both before and after all the trials by using the cognitive screening section of the adult version of SCAT5, which is the standardized assessment of concussion for clinical and academic research (McCrea, 2001). The cognitive screening section is comprised of three parts: (1) orientation, (2) immediate memory, and (3) concentration. The first part incudes 5 questions with one mark for correct answer to each question. The second part used for the study is split into two: two 5-word lists and one 10-word list, respectively, with one mark for each word remembered correctly. The third part includes a digit-list of 4 sets of digits with one mark for correctly identifying the reverse order of a set and one month-list with one mark for correctly identifying

the reverse order of the list. As such, the maximum total score is 5 for the orientation section, 10 and 5 for the two parts of the memory section, and 5 for the concentration section respectively.

For the assessment of participant recovery after all the trials, we computed the accuracy rate for an individual participant, defined as the total score of a section over the maximum total score for that section, for each of the three sections for the test conducted either before or after all the trials.

The average accuracy for the three different sections of the test before and after the trials are displayed by blue and orange bars respectively in Figure 5.3 where "O" is for the orientation section, "M1" and "M2" for the two parts of the immediate memory section, and "C" for the concentration section respectively. Clearly, the average accuracy before the trials did not exceed the average successful rate after the trials for all the sections. It should be noted that the SCAT-5 is not intended to diagnose concussion. Regardless, the results of this test provides evidence that there were no significant neurocognitive changes after the experiment.

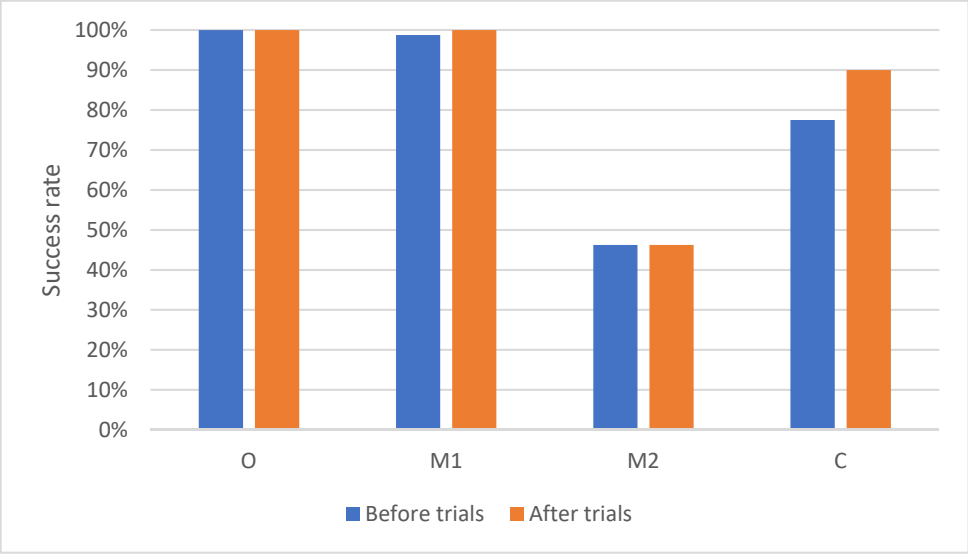

Figure 5.3 The average accuracy for the three sections of the concussion test after all the trials

In addition, we compared the difference in each of the four metrics between the two 5-minute resting states before and after trials separately by conducting a paired t-test with the null hypothesis of no difference in the metric and reported the results in Figures 5.4-5.7. There was no significant evidence of the change between the resting-states for either absolute or relative power. The findings suggested that the immediate power change due to heading may not have lasting or cumulative effects after the experiment. This result may explain why the EEG investigation on the effects of heading by Tysvaer et al. (1989) resulted in almost normal EEG recordings for the soccer players with concussion history in their study.

Furthermore, there was evidence of the change between the resting-states for both magnitude-squared and imaginary coherence in some of the bands. Specifically, the magnitude-squared coherence had an overall decrease from the pre to post resting-states while the imaginary coherence only had a significant decrease in the beta band. This finding was slightly different to those observed in the post-impact changes in magnitude-squared coherence. Perhaps the baseline coherence level has decreased overall during the experiments. The findings implied that the changes in the functional connectivity due to multiple consecutive heading may last longer than the changes in power.

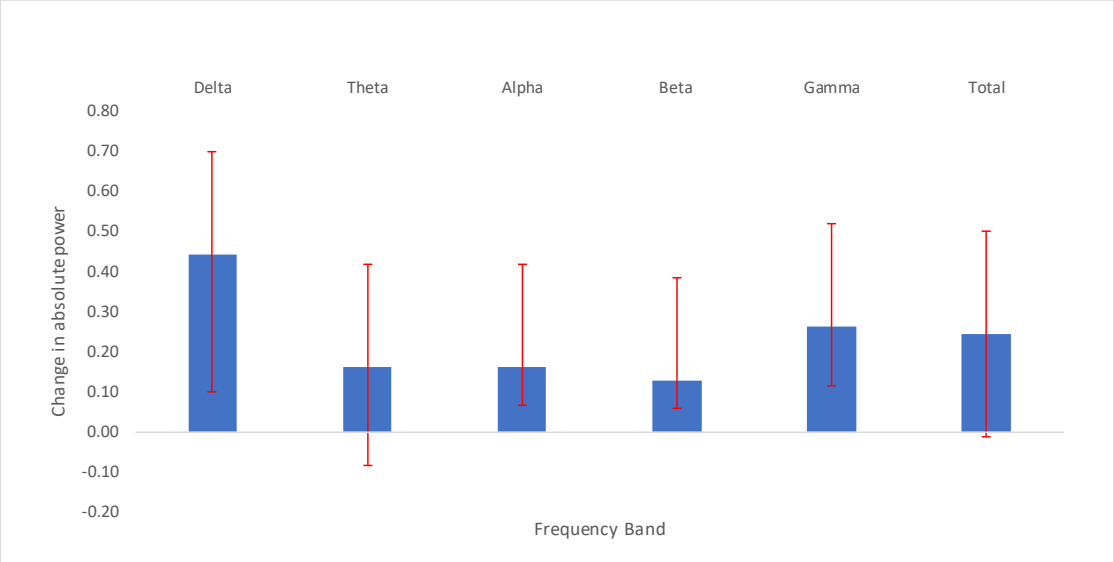

Figure 5.4 The average difference in absolute power between post and pre resting states.

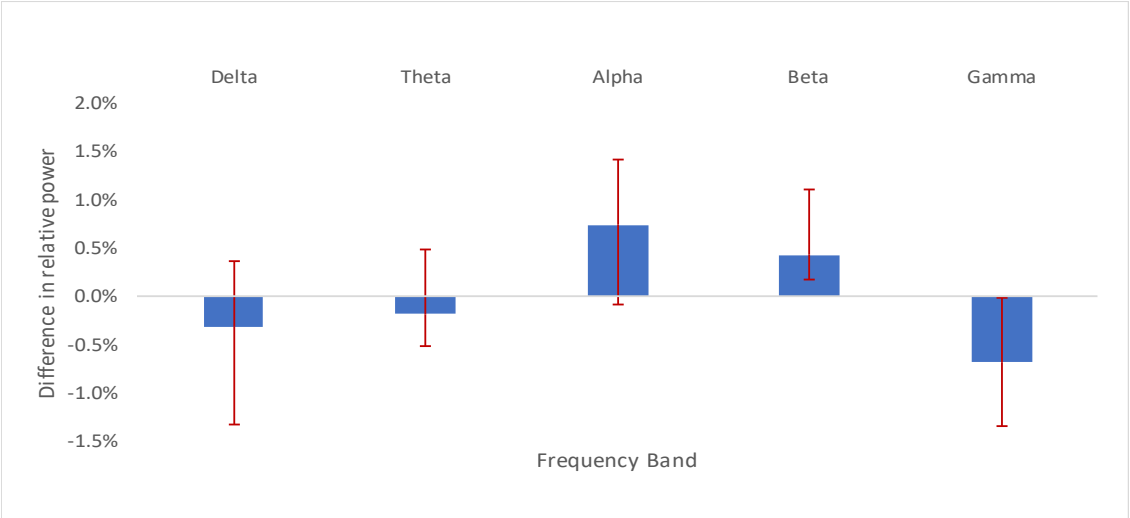

Figure 5.5 The average difference in relative power between pre-resting and post-resting states.

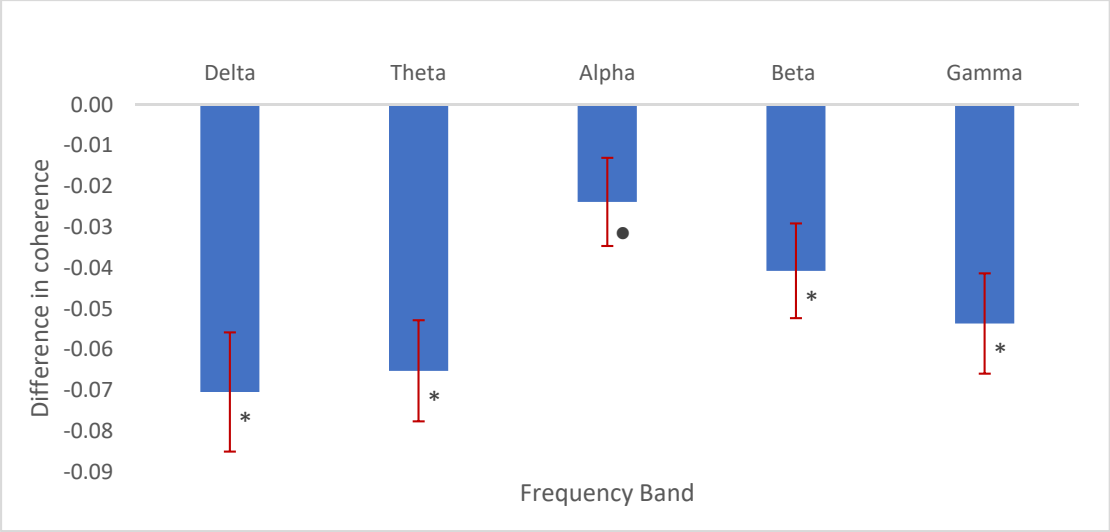

Figure 5.6 The average difference in magnitude squared coherence between pre- and post-resting states.
Note: ●, stands for the p-value of a test less than 0.05 and the threshold based on the Bonferroni correction respectively.*

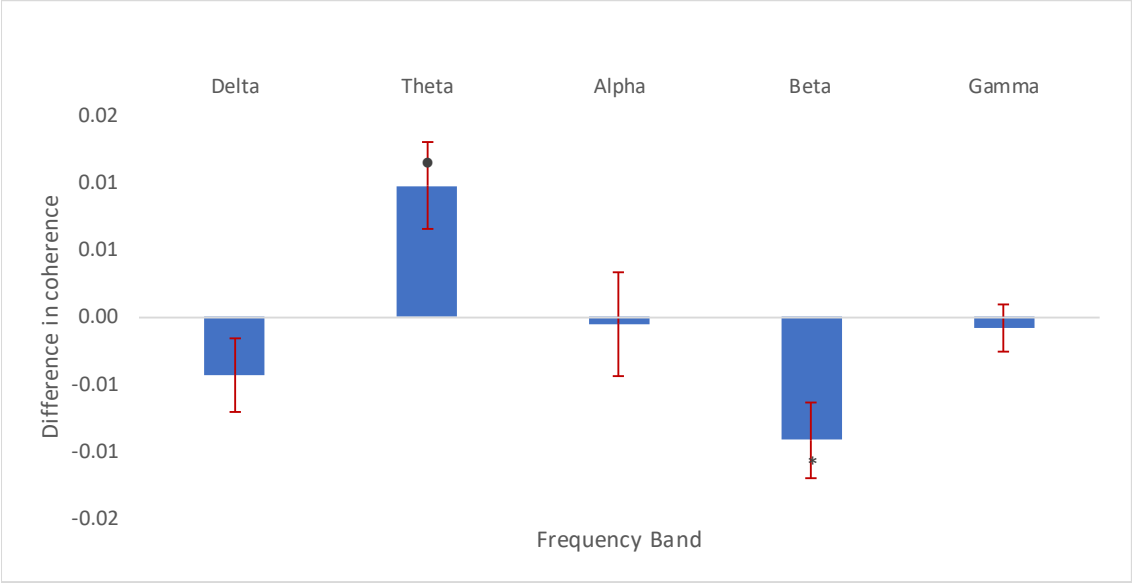

Figure 5.7 The average difference in imaginary coherence between post- and pre-resting states.
Note: ●, stand for the p-value of a test less than 0.05 and the threshold based on the Bonferroni correction respectively.*

Chapter 6: Conclusions

In this study, we designed and conducted a novel experiment to examine the immediate effects of controlled soccer headers by measuring EEG signals continuously during mild soccer headers. Through the experiment, we were able to determine whether the immediate effects of a mild soccer header on the brain can be detected with the use of EEG, and if these effects are affected by heading direction and ball speed. In this study, we observed immediate, transient changes in EEG signals lasting for seconds after mild soccer headers, indicating that the immediate effects of a mild soccer header on the brain could be detected with the use of EEG. More specifically, there was evidence of changes in both power and coherence due to heading based on the recorded EEG signals. For instance, there were an increase in absolute power due to heading across all the frequency bands and a decrease in magnitude squared coherence after the impact for theta band. We also found evidence that changes due to heading varied for different loading directions and ball speed, suggesting that the immediate effects of mild soccer header could be affected by ball direction and speed. Particularly, both ball direction and speed affected the changes in absolute power due to heading for all the bands but delta and the changes in magnitude squared coherence due to heading for the all bands respectively. Furthermore, for some of the frequency bands, changes in power were larger for side headers than for frontal headers and larger for high ball speed than for low ball speed. In addition, we found evidence of differences in the changes of EEG signals between sham headers and actual headers for some frequency bands in terms of each of the four metrics used in the study. Lastly, we found no evidence of changes in power between pre- and post-resting sessions, but some evidence of a decrease in coherence for some frequency bands after the trials.

To the best of our knowledge, our study was the first attempt of examining EEG signals in humans immediately after controlled soccer headers. Our findings indicated that potential transient effects of mild soccer headers could be measured sensitively and quantitatively with the use of EEG. Particularly, our findings on the ball speed with larger change in power for higher ball speed was consistent with the hypothesis that higher head kinematics, leading to higher brain deformations, are expected to result in greater neurophysiological changes. It is worth noting that some of the changes in power and coherence from our study resembled characteristic patterns found in previous studies on brain impairments in the literature. As such, more severe headers than those simulated in our experiments are anticipated to lead to greater but similar patterns of neurophysiological changes, and could potentially explain brain impairments resulting from these impacts. While our study was an exploratory analysis on the immediate effects of soccer headers with the use of EEG, our findings could serve as a stepping-stone in the efforts of investigating effects of various head impacts in sports.

Our study had several limitations. Firstly, the sample size in terms of number of participants in the experiment was small, which may limit our findings to being extrapolated widely. Secondly, the controlled headers performed in this study may not fully replicate on-field soccer headers. Specifically, in our experiment, the effective mass of the pendulum was much higher than the soccer ball, and the impact level of the headers and the location of the impact on the head were controlled. Consequently, there may be differences in impact dynamics between the controlled and on-field soccer headers. Thirdly, we have used a relatively sparse electrode setup which limited out coherence analysis and in-depth source localization analysis. Lastly, we are unable to analyze the EEG changes that occurred during the impact due to high levels of noise at the point of contact,

hence this thesis focuses on the data obtained when the head remained still immediately after the impact.

Our exploratory study has indicated the feasibility of using EEG to measure immediate effects of soccer headers. It has suggested at least two possible directions for future research in the field. One is to conduct more similar experiments with different designs and a larger number of participants to obtain more data on head impacts in sports. This includes the use of different EEG devices like wearable EEG and different types of participants. With cumulated information from this type of research, it may eventually lead to further development of screening technologies for head impact-related brain changes in clinical practice. The other direction is to explore how to use other biomedical imaging techniques together with EEG to analyze head impacts in sports. The aim of such research is to address whether and how head impacts in sports like soccer headers affect the structure and neurons in the brain, which may lead to better understanding on head impacts in sports.

Bibliography

[1] Acharya UR, Sree SV, Swapna G, Martis RJ, Suri JS. Automated EEG analysis of epilepsy: a review. Knowledge-Based Systems. 2013 Jun 1;45:147-65.

[2] Asken BM, Sullan MJ, DeKosky ST, Jaffee MS, Bauer RM. Research gaps and controversies in chronic traumatic encephalopathy: a review. JAMA neurology. 2017 Oct 1;74(10):1255-62.

[3] Aziezah F, Pratama SH, Wahidah E, Haryanto F. Characterization of Individual Alpha Frequency of EEG Signals as an Indicator of Cognitive Fatigue. InJournal of Physics: Conference Series 2020 Mar 1 (Vol. 1505, No. 1, p. 012068). IOP Publishing.

[4] Bai O, Lin P, Vorbach S, Floeter MK, Hattori N, Hallett M. A high performance sensorimotor beta rhythm-based brain–computer interface associated with human natural motor behavior. Journal of Neural Engineering. 2008; 5: 24–35.

[5] Barr WB, Prichep LS, Chabot R, Powell MR, McCrea M. Measuring brain electrical activity to track recovery from sport-related concussion. Brain injury. 2012 Jan 1;26(1):58-66.

[6] Baumeister J, Reinecke K, Liesen H, Weiss M. Cortical activity of skilled performance in a complex sports related motor task. European Journal of Applied Physiology. 2008 Jul; 104:625–631.

[7] Bowyer SM. Coherence a measure of the brain networks: past and present. Neuropsychiatric Electrophysiology. 2016 Dec 1;2(1):1.

[8] Broglio SP, Guskiewicz KM, Sell TC, Lephart SM. No acute changes in postural control after soccer heading. British Journal of Sports Medicine. 2004 Oct 1;38(5):561-7.

[9] Buschman TJ, Denovellis EL, Diogo C, Bullock D, Miller EK. Synchronous oscillatory neural ensembles for rules in the prefrontal cortex. Neuron. 2012 Nov;76 (4): 838-846.

[10] Cantu RC. Cerebral concussion in sport. Sports Medicine. 1992 Jul 1;14(1):64-74.

[11] Coenen A, Fine E, Zaychkivska O. Adolf Beck: A forgotten pioneer in Electroencephalography. Journal of the History of the Neurosciences. 2014 23:276–286.

[12] Guggisberg AG, Dalal SS, Zumer JM, Wong DD, Dubovik S, Michel CM, Schnider A. Localization of cortico-peripheral coherence with electroencephalography. Neuroimage. 2011 Aug 15;57(4):1348-57.

[13] Guskiewicz KM, Marshall SW, Broglio SP, Cantu RC, Kirkendall DT. No evidence of impaired neurocognitive performance in collegiate soccer players. The American Journal of Sports Medicine. 2002 Mar;30(2):157-62.

[14] Ho MC, Chen TC, Huang CF, Yu CH, Chen JM, Huang RY, Ho HC, Liu CJ. Detect AD patients by using EEG coherence analysis. Journal of Medical Engineering, 2014, Feb; 2014 236734.

[15] Homan RW, Herman J, Purdy P. Cerebral location of international 10–20 system electrode placement. Electroencephalography and clinical neurophysiology. 1987 Apr 1;66(4):376-82.

[16] Huber PJ. Robust Statistics. New York, NY: Wiley. 1980.

[17] Joy JE, Patlak M. Is soccer bad for children's heads? Summary of the IOM Workshop on Neuropsychological Consequences of Head Impact in Youth Soccer. National Academies Press; 2002 Apr 29.

[18] Jordan SE, Green GA, Galanty HL, Mandelbaum BR, Jabour BA. Acute and chronic brain injury in United States National Team soccer players. The American Journal of Sports Medicine. 1996 Mar;24(2):205-10.

[19] Kirschstein T, Köhling R. What is the source of the EEG?. Clinical EEG and neuroscience. 2009 Jul;40(3):146-9.

[20] Korn A, Golan H, Melamed I, Pascual-Marqui R, Friedman A. Focal cortical dysfunction and blood–brain barrier disruption in patients with postconcussion syndrome. Journal of Clinical Neurophysiology, 2005 Feb; 22(1):1-9.

[21] Koutures CG, Gregory AJ. Injuries in youth soccer. Pediatrics. 2010 Feb 1;125(2):410-4.

[22] Kross R, Ohler K, Barolin GS. Cerebral Trauma due to heading—Computerized EEG-analysis of football players. EEG-EMG 14: 209–212.

[23] Kuo C, Fanton M, Wu L, Camarillo D. Spinal constraint modulates head instantaneous center of rotation and dictates head angular motion. Journal of Biomechanics. 2018 Jul 25;76: 220-228.

[24] Locatelli T, Cursi M, Liberati D, Franceschi M, Comi G. EEG coherence in Alzheimer's disease. Electroencephalography and Clinical Neurophysiology. 1998 Mar 1;106(3):229-37.

[25] Lopez-Moreno I, Gonzalez-Dominguez J, Plchot O, Martinez D, Gonzalez-Rodriguez J, Moreno P. Automatic language identification using deep neural networks. In2014 IEEE international conference on acoustics, speech and signal processing (ICASSP) 2014 May 4 (pp. 5337-5341). IEEE.

[26] Machado S, Portella CE, Silva JG, Velasques B. Terra P, Vorkapic CF, da Silva VF, Miana L, Basile L. Cagy M, Piedade R, Ribeiro P. Changes in quantitative EEG absolute power during the task of catching an object in free fall. Arq Neuropsiquiatr, 2007; 65(3-A):633-636.

[27] Matser EJ, Kessels AG, Lezak MD, Jordan BD, Troost J. Neuropsychological impairment in amateur soccer players. The Journal of the American Medical Association. 1999 Sep 8;282(10):971-3.

[28] Matser JT, Kessels AG, Jordan BD, Lezak MD, Troost J. Chronic traumatic brain injury in professional soccer players. Neurology. 1998 Sep 1;51(3):791-6.

[29] McCrea M. Standardized mental status testing of acute concussion. Clinical Journal of Sport Medicine. 2001; 11: 176-181.

[30] Miller LE, Urban JE, Kelley ME, Powers AK, Whitlow CT, Maldjian JA, Rowson S, Stitzel JD. Evaluation of brain response during head impact in youth athletes using an anatomically accurate finite element model. Journal of neurotrauma. 2019 May 15;36(10):1561-70.

[31] Newson JJ, Tiagarajan TC. EEG Frequency Bands in Psychiatric Disorders: A Review of Resting State Studies. Frontiers in Human Neuroscience. 2019 Jan; 12 (Article 521):1-24.

[32] Nolte G, Bai O, Wheaton L, Mari Z, Vorbach S, Hallett M. Identifying true brain interaction from EEG data using the imaginary part of coherency. Clinical Neurophysiology. 2004 Oct 1;115(10):2292-307.

[33] Nunez PL, Srinivasan R. Electric fields of the brain: the neurophysics of EEG. Oxford University Press, USA; 2006.

[34] Nuwer MR, Hovdac DA, Schradera LM, Vespa PM. Routine and quantitative EEG in mild traumatic brain injury. Clinical Neurophysiology. 2005; 116:2001–2025

[35] Oldrich V, Jaromir K, Ales P, Pazdera L, Simko, J, Valis M. Age-related changes in EEG coherence. Neurologia i Neurochirurgia Polska, 2014 Jan-Feb; 48(1):35-38.

[36] Olejniczak P. Neurophysiologic basis of EEG. Journal of clinical neurophysiology. 2006 Jun 1;23(3):186-9.

[37] Patlak M, Joy JE, Board on Neuroscience and Behavioral Health. Is soccer bad for children's heads? summary of the IOM Workshop on Neuropsychological Con- sequences of Head Impact in Youth Soccer. Washington, DC: National Academies Press, 2002.

[38] Poltavski D, Bernhardt K, Mark C, Biberdor D. Frontal theta-gamma ratio is a sensitive index of concussion history in athletes on tasks of visuomotor control. Scientific Reports, 2019; 9:17565.

[39] Sander TH, Bock A, Leistner S, K¨uhn A, Trahms L. Coherence and imaginary part of coherency identifies cortico-muscular and cortico-thalamic coupling. 32nd Annual International Conference of the IEEE EMBS, Buenos Aires, Argentina, 2010 August 31 - September 4.

[40] Santamaria I, Via J. Estimation of the magnitude squared coherence spectrum based on reduced-rank canonical coordinates. In2007 IEEE International Conference on Acoustics, Speech and Signal Processing-ICASSP'07 2007 Apr 15 (Vol. 3, pp. III-985). IEEE.

[41] Singh KD. Which "neural activity" do you mean? fMRI, MEG, oscillations and neurotransmitters. NeuroImage. 2012 Aug; 62(2):1121-1130.

[42] Slobounov SM, Sebastianelli W. Concussions in athletics. Springer-Verlag New York; 2016.

[43] Slobounov S, Sebastianelli W, Hallett M. Residual brain dysfunction observed one year post-mild traumatic brain injury: combined EEG and balance study. Clinical Neurophysiology. 2012 Sep 1;123(9):1755-61.

[44] Sortland O, Tysvaer AT. Brain damage in former association football players. Neuroradiology. 1989 Mar 1;31(1):44-8.

[45] Spiotta AM, Bartsch AJ, Benzel EC. Heading in soccer: dangerous play? Neurosurgery. 2012 Jan 1;70(1):1-1.

[46] Thatcher RW, Krause PJ, Hrybyk M. Cortico-cortical associations and EEG coherence: a two-compartmental model. Electroencephalography and clinical neurophysiology. 1986 Aug 1;64(2):123-43.

[47] Thatcher RW, Walker RA, Gerson I, Geisler FH. EEG discriminant analyses of mild head trauma. Electroencephalography and clinical neurophysiology. 1989 Aug 1;73(2):94-106.

[48] Thatcher RW. Validity and reliability of quantitative electroencephalography. Journal of Neurotherapy. 2010 May 20;14(2):122-52.

[49] Tomkins O, Feintuch A, Benifla M, Cohen A, Friedman A, Shelef I. Blood-brain barrier breakdown following traumatic brain injury: a possible role in posttraumatic epilepsy. Cardiovascular Psychiatry and Neurology. 2011 Feb; (2090-0163):765923.

[50] Thompson J, Sebastianelli W, Slobounov, S. EEG and postural correlates of mild traumatic brain injury in athletes. Neuroscience Letters. 2005; 377:158–163

[51] Tysvaer AT, Løchen EA. Soccer injuries to the brain: a neuropsychologic study of former soccer players. The American Journal of Sports Medicine. 1991 Jan;19(1):56-60.

[52] Tysvaer AT, Storli OV, Bachen NI. Soccer injuries to the brain. A neurologic and electroencephalographic study of former players. Acta Neurologica Scandinavica. 1989 Aug; 80(2):151-6.

[53] Uddin LQ. Complex relationships between structural and functional brain connectivity. Trends in Cognitive Sciences. 2013 Dec 1;17(12):600-2.

[54] Vladimir M, Andreas K. Reliability of event-related EEG functional connectivity during visual entrainment: Magnitude squared coherence and phase synchrony estimates. Psychophysiology, 2015; vol. 52,81-89.

[55] Welch P. The use of fast Fourier transform for the estimation of power spectra: a method based on time averaging over short, modified periodograms. IEEE Transactions on audio and electroacoustics. 1967 Jun;15(2):70-3.

Appendix A: Pre- and Post-Heading Statistics with Loading Direction and Speed

Pre- and Post-Heading Statistics with Loading Direction and Speed for Relative Power

(P-value is for t-test with hull hypothesis of mean of post-heading over pre-heading equal to zero.)

Statistics	Soft Speed			Hard Speed		
	Front Loading	Left Loading	Right Loading	Front Loading	Left Loading	Right Loading
Delta						
Mean (pre-heading)	0.466	0.453	0.515	0.437	0.499	0.510
Mean(post-heading)	0.523	0.532	0.561	0.530	0.569	0.565
Mean(after-before)	0.057	0.079	0.046	0.093	0.071	0.055
P-value	0.000	0.000	0.000	0.000	0.000	0.000
Theta						
Mean (pre-heading)	0.180	0.167	0.185	0.152	0.163	0.177
Mean(post-heading)	0.161	0.129	0.152	0.141	0.156	0.152
Mean(after-before)	-0.019	-0.038	-0.034	-0.011	-0.007	-0.024
P-value	0.021	0.000	0.000	0.079	0.133	0.000
Alpha						
Mean (pre-heading)	0.172	0.173	0.156	0.154	0.141	0.128
Mean(post-heading)	0.133	0.138	0.142	0.135	0.115	0.101
Mean(after-before)	-0.039	-0.035	-0.014	-0.019	-0.026	-0.027
P-value	0.000	0.000	0.065	0.002	0.000	0.000
Beta						
Mean (pre-heading)	0.124	0.127	0.113	0.146	0.124	0.117
Mean(post-heading)	0.119	0.111	0.102	0.121	0.100	0.113
Mean(after-before)	-0.005	-0.016	-0.011	-0.025	-0.024	-0.004
P-value	0.218	0.000	0.003	0.000	0.000	0.347
Gamma						
Mean (pre-heading)	0.153	0.179	0.131	0.198	0.165	0.165
Mean(post-heading)	0.155	0.168	0.130	0.153	0.146	0.155
Mean(after-before)	0.003	-0.011	0.000	-0.046	-0.019	-0.010
P-value	0.679	0.115	0.943	0.000	0.005	0.065

Pre- and Post-Heading Statistics with Loading Direction and Speed for Absolute Power

(P-value is for t-test with hull hypothesis of mean of post-heading over pre-heading equal to zero.)

Statistics	4 rad/s			7 rad/s		
	Front Loading	Left Loading	Right Loading	Front Loading	Left Loading	Right Loading
Delta						
Mean (pre-heading)	1.332	1.455	1.570	1.020	1.995	2.388
Mean(post-heading)	2.091	18.613	6.327	6.468	4.564	30.264
Mean(after-before)	0.759	17.158	4.757	5.448	2.569	27.875
P-value	0.098	0.000	0.002	0.005	0.035	0.000
Theta						
Mean (pre-heading)	1.714	2.541	1.731	1.404	3.295	4.084
Mean(post-heading)	1.343	2.129	2.077	3.396	6.270	6.769
Mean(after-before)	-0.371	-0.412	0.345	1.992	2.976	2.684
P-value	0.052	0.118	0.065	0.010	0.001	0.124
Alpha						
Mean (pre-heading)	1.662	3.104	2.239	2.342	2.439	2.842
Mean(post-heading)	1.454	3.127	2.586	3.238	5.243	4.845
Mean(after-before)	-0.208	0.022	0.347	0.897	2.804	2.003
P-value	0.089	0.964	0.051	0.134	0.000	0.033
Beta						
Mean (pre-heading)	1.562	2.682	2.151	2.221	2.027	2.741
Mean(post-heading)	1.442	3.558	2.303	3.442	5.252	5.476
Mean(after-before)	-0.120	0.876	0.152	1.221	3.225	2.735
P-value	0.355	0.000	0.360	0.000	0.000	0.011
Gamma						
Mean (pre-heading)	1.553	2.742	1.457	2.196	2.250	2.750
Mean(post-heading)	1.338	4.334	1.849	3.241	3.964	4.134
Mean(after-before)	-0.214	1.592	0.392	1.045	1.714	1.384
P-value	0.214	0.000	0.000	0.000	0.000	0.005
Total						
Mean (pre-heading)	1.208	1.775	1.396	1.072	1.810	2.178
Mean(post-heading)	1.559	11.111	4.055	4.634	3.703	17.500
Mean(after-before)	0.351	9.336	2.659	3.562	1.893	15.322
P-value	0.205	0.000	0.003	0.004	0.009	0.000

Pre- and Post-Heading Statistics with Loading Direction, Speed and Electrode Group for Magnitude Squared Coherence

(P-value is for t-test with hull hypothesis of mean of post-heading over pre-heading equal to zero.)

Delta							
Electrode Location	Statistics	4 rad/s			7 rad/s		
		Front Loading	Left Loading	Right Loading	Front Loading	Left Loading	Right Loading
F3(1)	Mean (pre-heading)	0.668	0.655	0.649	0.564	0.617	0.607
	Mean(post-heading)	0.645	0.659	0.590	0.568	0.568	0.612
	Mean(after-before)	-0.024	0.004	-0.060	0.003	-0.049	0.005
	P-value	0.356	0.847	0.006	0.892	0.038	0.855
F3(2)	Mean (pre-heading)	0.703	0.660	0.658	0.633	0.633	0.721
	Mean(post-heading)	0.718	0.658	0.647	0.642	0.601	0.691
	Mean(after-before)	0.014	-0.002	-0.011	0.009	-0.033	-0.030
	P-value	0.401	0.922	0.569	0.643	0.274	0.201
F3(3)	Mean (pre-heading)	0.473	0.440	0.419	0.385	0.371	0.448
	Mean(post-heading)	0.485	0.468	0.434	0.434	0.378	0.454
	Mean(after-before)	0.012	0.028	0.015	0.049	0.007	0.006
	P-value	0.392	0.026	0.305	0.002	0.673	0.799
F3(4)	Mean (pre-heading)	0.533	0.509	0.444	0.384	0.486	0.490
	Mean(post-heading)	0.496	0.515	0.334	0.414	0.410	0.497
	Mean(after-before)	-0.037	0.006	-0.110	0.029	-0.075	0.008
	P-value	0.295	0.842	0.000	0.479	0.018	0.802
F3(5)	Mean (pre-heading)	0.631	0.523	0.544	0.577	0.569	0.669
	Mean(post-heading)	0.658	0.543	0.533	0.565	0.499	0.618
	Mean(after-before)	0.027	0.020	-0.011	-0.012	-0.070	-0.050
	P-value	0.243	0.420	0.588	0.694	0.033	0.186
F3(6)	Mean (pre-heading)	0.483	0.462	0.382	0.348	0.380	0.418
	Mean(post-heading)	0.473	0.438	0.340	0.382	0.354	0.448
	Mean(after-before)	-0.010	-0.024	-0.042	0.034	-0.026	0.030
	P-value	0.823	0.543	0.254	0.456	0.432	0.508
F3(7)	Mean (pre-heading)	0.481	0.335	0.346	0.387	0.418	0.496
	Mean(post-heading)	0.520	0.362	0.339	0.454	0.354	0.477
	Mean(after-before)	0.039	0.027	-0.007	0.067	-0.064	-0.019
	P-value	0.365	0.370	0.835	0.144	0.040	0.784
F3(8)	Mean (pre-heading)	0.486	0.375	0.315	0.329	0.289	0.339
	Mean(post-heading)	0.472	0.377	0.308	0.337	0.274	0.349
	Mean(after-before)	-0.014	0.002	-0.007	0.007	-0.015	0.011
	P-value	0.717	0.966	0.792	0.773	0.553	0.851

Theta							
Electrode Location	Statistics	4 rad/s			7 rad/s		
		Front Loading	Left Loading	Right Loading	Front Loading	Left Loading	Right Loading
F3(1)	Mean (pre-heading)	0.656	0.633	0.633	0.538	0.599	0.581
	Mean(post-heading)	0.647	0.602	0.579	0.572	0.554	0.581
	Mean(after-before)	-0.009	-0.031	-0.054	0.033	-0.045	0.000
	P-value	0.443	0.002	0.000	0.046	0.004	0.977
F3(2)	Mean (pre-heading)	0.687	0.596	0.659	0.587	0.590	0.679
	Mean(post-heading)	0.653	0.593	0.606	0.601	0.536	0.658
	Mean(after-before)	-0.033	-0.002	-0.053	0.014	-0.053	-0.021
	P-value	0.006	0.877	0.000	0.371	0.004	0.263
F3(3)	Mean (pre-heading)	0.430	0.385	0.406	0.322	0.310	0.383
	Mean(post-heading)	0.419	0.369	0.381	0.378	0.315	0.380
	Mean(after-before)	-0.011	-0.016	-0.025	0.056	0.005	-0.003
	P-value	0.162	0.080	0.003	0.000	0.564	0.826
F3(4)	Mean (pre-heading)	0.466	0.489	0.394	0.353	0.464	0.465
	Mean(post-heading)	0.445	0.435	0.316	0.343	0.399	0.446
	Mean(after-before)	-0.021	-0.054	-0.078	-0.010	-0.065	-0.018
	P-value	0.229	0.001	0.000	0.597	0.000	0.273
F3(5)	Mean (pre-heading)	0.612	0.457	0.536	0.527	0.493	0.618
	Mean(post-heading)	0.587	0.480	0.480	0.515	0.420	0.600
	Mean(after-before)	-0.026	0.023	-0.056	-0.012	-0.073	-0.018
	P-value	0.084	0.155	0.001	0.543	0.002	0.514
F3(6)	Mean (pre-heading)	0.463	0.426	0.375	0.354	0.324	0.389
	Mean(post-heading)	0.432	0.383	0.323	0.335	0.328	0.385
	Mean(after-before)	-0.031	-0.043	-0.052	-0.018	0.004	-0.004
	P-value	0.206	0.039	0.001	0.496	0.888	0.841
F3(7)	Mean (pre-heading)	0.412	0.275	0.318	0.278	0.296	0.426
	Mean(post-heading)	0.407	0.270	0.300	0.340	0.279	0.412
	Mean(after-before)	-0.006	-0.005	-0.018	0.062	-0.016	-0.014
	P-value	0.711	0.858	0.315	0.023	0.375	0.727
F3(8)	Mean (pre-heading)	0.447	0.339	0.313	0.334	0.220	0.283
	Mean(post-heading)	0.417	0.302	0.275	0.315	0.235	0.305
	Mean(after-before)	-0.031	-0.036	-0.039	-0.019	0.014	0.023
	P-value	0.229	0.182	0.019	0.417	0.415	0.333

Alpha							
Electrode Location	Statistics	4 rad/s			7 rad/s		
		Front Loading	Left Loading	Right Loading	Front Loading	Left Loading	Right Loading
F3(1)	Mean (pre-heading)	0.654	0.611	0.615	0.541	0.553	0.525
	Mean(post-heading)	0.642	0.600	0.612	0.586	0.552	0.534
	Mean(after-before)	-0.012	-0.011	-0.002	0.045	-0.001	0.009
	P-value	0.352	0.448	0.871	0.009	0.928	0.542
F3(2)	Mean (pre-heading)	0.638	0.553	0.589	0.575	0.565	0.635
	Mean(post-heading)	0.634	0.570	0.571	0.583	0.531	0.608
	Mean(after-before)	-0.004	0.016	-0.019	0.009	-0.034	-0.026
	P-value	0.769	0.304	0.198	0.585	0.034	0.099
F3(3)	Mean (pre-heading)	0.393	0.344	0.364	0.329	0.292	0.340
	Mean(post-heading)	0.397	0.373	0.375	0.391	0.311	0.321
	Mean(after-before)	0.004	0.029	0.011	0.061	0.019	-0.019
	P-value	0.686	0.003	0.343	0.000	0.057	0.036
F3(4)	Mean (pre-heading)	0.435	0.457	0.379	0.356	0.433	0.449
	Mean(post-heading)	0.424	0.437	0.366	0.380	0.391	0.402
	Mean(after-before)	-0.011	-0.019	-0.013	0.024	-0.042	-0.048
	P-value	0.473	0.174	0.498	0.274	0.088	0.001
F3(5)	Mean (pre-heading)	0.561	0.419	0.456	0.520	0.494	0.558
	Mean(post-heading)	0.590	0.473	0.454	0.521	0.415	0.548
	Mean(after-before)	0.030	0.054	-0.002	0.001	-0.078	-0.010
	P-value	0.098	0.003	0.900	0.966	0.001	0.508
F3(6)	Mean (pre-heading)	0.432	0.394	0.364	0.379	0.319	0.393
	Mean(post-heading)	0.412	0.412	0.329	0.393	0.309	0.350
	Mean(after-before)	-0.020	0.018	-0.035	0.014	-0.010	-0.043
	P-value	0.332	0.336	0.040	0.611	0.776	0.081
F3(7)	Mean (pre-heading)	0.345	0.231	0.259	0.265	0.274	0.367
	Mean(post-heading)	0.400	0.293	0.313	0.339	0.254	0.329
	Mean(after-before)	0.055	0.062	0.054	0.074	-0.020	-0.039
	P-value	0.016	0.032	0.049	0.019	0.420	0.117
F3(8)	Mean (pre-heading)	0.399	0.320	0.262	0.364	0.234	0.296
	Mean(post-heading)	0.409	0.318	0.290	0.379	0.247	0.242
	Mean(after-before)	0.010	-0.003	0.028	0.014	0.013	-0.053
	P-value	0.529	0.900	0.246	0.655	0.689	0.022

Beta							
Electrode Location	Statistics	4 rad/s			7 rad/s		
		Front Loading	Left Loading	Right Loading	Front Loading	Left Loading	Right Loading
F3(1)	Mean (pre-heading)	0.616	0.564	0.560	0.525	0.535	0.507
	Mean(post-heading)	0.594	0.575	0.560	0.553	0.531	0.518
	Mean(after-before)	-0.022	0.010	0.000	0.028	-0.004	0.011
	P-value	0.080	0.251	0.997	0.087	0.796	0.372
F3(2)	Mean (pre-heading)	0.623	0.555	0.540	0.568	0.544	0.615
	Mean(post-heading)	0.620	0.552	0.566	0.560	0.528	0.590
	Mean(after-before)	-0.004	-0.003	0.027	-0.008	-0.016	-0.025
	P-value	0.694	0.746	0.030	0.572	0.211	0.062
F3(3)	Mean (pre-heading)	0.391	0.327	0.315	0.328	0.297	0.313
	Mean(post-heading)	0.378	0.351	0.346	0.362	0.314	0.304
	Mean(after-before)	-0.013	0.024	0.031	0.034	0.017	-0.009
	P-value	0.051	0.000	0.000	0.002	0.011	0.266
F3(4)	Mean (pre-heading)	0.429	0.389	0.328	0.311	0.394	0.383
	Mean(post-heading)	0.377	0.395	0.308	0.349	0.372	0.352
	Mean(after-before)	-0.052	0.005	-0.020	0.039	-0.022	-0.031
	P-value	0.009	0.590	0.079	0.038	0.351	0.017
F3(5)	Mean (pre-heading)	0.561	0.428	0.417	0.510	0.455	0.544
	Mean(post-heading)	0.578	0.450	0.466	0.521	0.442	0.547
	Mean(after-before)	0.017	0.022	0.049	0.011	-0.013	0.004
	P-value	0.174	0.068	0.001	0.638	0.314	0.856
F3(6)	Mean (pre-heading)	0.415	0.355	0.317	0.332	0.338	0.330
	Mean(post-heading)	0.344	0.376	0.285	0.358	0.314	0.315
	Mean(after-before)	-0.071	0.021	-0.032	0.026	-0.025	-0.015
	P-value	0.002	0.169	0.060	0.222	0.229	0.359
F3(7)	Mean (pre-heading)	0.372	0.247	0.239	0.294	0.263	0.341
	Mean(post-heading)	0.385	0.281	0.301	0.337	0.272	0.332
	Mean(after-before)	0.012	0.034	0.063	0.043	0.009	-0.009
	P-value	0.571	0.055	0.006	0.195	0.578	0.669
F3(8)	Mean (pre-heading)	0.375	0.298	0.227	0.317	0.248	0.248
	Mean(post-heading)	0.353	0.305	0.253	0.342	0.248	0.226
	Mean(after-before)	-0.022	0.007	0.026	0.025	0.001	-0.021
	P-value	0.292	0.703	0.031	0.163	0.975	0.261

Gamma							
Electrode Location	Statistics	4 rad/s			7 rad/s		
		Front Loading	Left Loading	Right Loading	Front Loading	Left Loading	Right Loading
F3(1)	Mean (pre-heading)	0.588	0.564	0.525	0.526	0.527	0.512
	Mean(post-heading)	0.572	0.562	0.527	0.538	0.521	0.506
	Mean(after-before)	-0.016	-0.002	0.002	0.013	-0.007	-0.005
	P-value	0.140	0.755	0.828	0.255	0.636	0.561
F3(2)	Mean (pre-heading)	0.651	0.613	0.588	0.622	0.594	0.641
	Mean(post-heading)	0.642	0.604	0.589	0.593	0.565	0.644
	Mean(after-before)	-0.009	-0.008	0.001	-0.028	-0.028	0.003
	P-value	0.369	0.385	0.931	0.058	0.017	0.847
F3(3)	Mean (pre-heading)	0.420	0.373	0.337	0.373	0.355	0.344
	Mean(post-heading)	0.407	0.372	0.356	0.379	0.331	0.349
	Mean(after-before)	-0.013	-0.001	0.019	0.006	-0.024	0.005
	P-value	0.051	0.801	0.017	0.427	0.006	0.576
F3(4)	Mean (pre-heading)	0.406	0.401	0.284	0.292	0.390	0.372
	Mean(post-heading)	0.366	0.387	0.315	0.327	0.358	0.337
	Mean(after-before)	-0.040	-0.014	0.031	0.035	-0.032	-0.035
	P-value	0.027	0.076	0.009	0.059	0.109	0.072
F3(5)	Mean (pre-heading)	0.594	0.508	0.476	0.548	0.511	0.572
	Mean(post-heading)	0.601	0.492	0.491	0.555	0.491	0.588
	Mean(after-before)	0.008	-0.016	0.015	0.007	-0.020	0.017
	P-value	0.564	0.221	0.225	0.529	0.055	0.370
F3(6)	Mean (pre-heading)	0.392	0.357	0.246	0.299	0.355	0.327
	Mean(post-heading)	0.357	0.343	0.288	0.331	0.317	0.291
	Mean(after-before)	-0.035	-0.014	0.042	0.033	-0.038	-0.036
	P-value	0.152	0.330	0.002	0.110	0.210	0.183
F3(7)	Mean (pre-heading)	0.407	0.330	0.294	0.354	0.347	0.407
	Mean(post-heading)	0.399	0.332	0.310	0.387	0.316	0.406
	Mean(after-before)	-0.008	0.002	0.016	0.033	-0.031	-0.001
	P-value	0.758	0.888	0.397	0.027	0.051	0.949
F3(8)	Mean (pre-heading)	0.360	0.303	0.210	0.286	0.276	0.228
	Mean(post-heading)	0.362	0.304	0.231	0.298	0.267	0.233
	Mean(after-before)	0.002	0.000	0.021	0.012	-0.009	0.005
	P-value	0.940	0.983	0.156	0.439	0.590	0.683

Pre- and Post- Heading Statistics with Loading Direction, Speed and Electrode Group for Magnitude Squared Coherence

(P-value is for t-test with hull hypothesis of mean of post-heading over pre-heading equal to zero.)

Delta							
Electrode Location	Statistics	4 rad/s			7 rad/s		
		Front Loading	Left Loading	Right Loading	Front Loading	Left Loading	Right Loading
F3(1)	Mean (pre-heading)	0.010	0.011	0.003	-0.012	-0.032	-0.010
	Mean(post-heading)	0.000	-0.004	0.016	-0.007	0.020	0.023
	Mean(after-before)	-0.009	-0.015	0.012	0.005	0.052	0.033
	P-value	0.648	0.398	0.577	0.861	0.040	0.163
F3(2)	Mean (pre-heading)	-0.031	-0.042	-0.008	-0.008	-0.021	-0.006
	Mean(post-heading)	-0.027	-0.030	-0.012	0.004	-0.028	-0.031
	Mean(after-before)	0.003	0.011	-0.005	0.012	-0.006	-0.026
	P-value	0.885	0.576	0.833	0.610	0.816	0.400
F3(3)	Mean (pre-heading)	0.016	-0.024	-0.005	-0.016	-0.025	-0.030
	Mean(post-heading)	-0.015	-0.017	-0.020	-0.006	0.014	0.023
	Mean(after-before)	-0.031	0.006	-0.015	0.009	0.040	0.052
	P-value	0.092	0.681	0.410	0.657	0.094	0.013
F3(4)	Mean (pre-heading)	-0.058	-0.015	0.042	0.046	-0.040	-0.002
	Mean(post-heading)	0.018	0.006	0.046	-0.030	-0.050	0.051
	Mean(after-before)	0.076	0.021	0.004	-0.076	-0.011	0.053
	P-value	0.018	0.337	0.922	0.095	0.730	0.104
F3(5)	Mean (pre-heading)	0.020	-0.116	-0.059	0.010	-0.037	-0.039
	Mean(post-heading)	-0.027	-0.033	-0.046	-0.004	-0.066	-0.016
	Mean(after-before)	-0.048	0.083	0.013	-0.014	-0.028	0.024
	P-value	0.038	0.009	0.687	0.550	0.401	0.453
F3(6)	Mean (pre-heading)	-0.052	-0.020	0.015	0.009	-0.016	-0.031
	Mean(post-heading)	-0.013	-0.006	0.008	-0.034	-0.040	0.013
	Mean(after-before)	0.039	0.014	-0.008	-0.043	-0.024	0.045
	P-value	0.357	0.693	0.900	0.535	0.712	0.269
F3(7)	Mean (pre-heading)	0.060	-0.113	-0.063	-0.074	-0.032	-0.032
	Mean(post-heading)	-0.026	-0.049	-0.037	-0.027	-0.051	0.019
	Mean(after-before)	-0.087	0.064	0.026	0.046	-0.018	0.051
	P-value	0.085	0.203	0.471	0.309	0.762	0.242
F3(8)	Mean (pre-heading)	-0.029	-0.041	-0.065	-0.024	-0.060	-0.027
	Mean(post-heading)	-0.043	-0.054	-0.015	-0.046	-0.091	0.036
	Mean(after-before)	-0.014	-0.012	0.050	-0.022	-0.031	0.063
	P-value	0.561	0.747	0.137	0.692	0.588	0.187

Theta							
Electrode Location	Statistics	4 rad/s			7 rad/s		
		Front Loading	Left Loading	Right Loading	Front Loading	Left Loading	Right Loading
F3(1)	Mean (pre-heading)	0.015	-0.006	0.004	-0.014	-0.015	0.002
	Mean(post-heading)	0.017	0.003	0.005	-0.009	0.000	0.012
	Mean(after-before)	0.002	0.009	0.001	0.005	0.015	0.011
	P-value	0.904	0.631	0.959	0.810	0.558	0.754
F3(2)	Mean (pre-heading)	-0.002	-0.043	-0.006	-0.023	-0.007	-0.010
	Mean(post-heading)	0.004	-0.032	-0.012	0.008	0.005	-0.013
	Mean(after-before)	0.006	0.011	-0.006	0.031	0.012	-0.003
	P-value	0.761	0.511	0.790	0.159	0.680	0.932
F3(3)	Mean (pre-heading)	-0.013	-0.030	0.021	0.027	0.019	0.010
	Mean(post-heading)	0.004	-0.016	0.033	0.003	0.014	0.044
	Mean(after-before)	0.017	0.014	0.012	-0.024	-0.004	0.034
	P-value	0.315	0.315	0.495	0.131	0.796	0.180
F3(4)	Mean (pre-heading)	-0.038	-0.013	0.078	0.060	-0.048	0.015
	Mean(post-heading)	0.080	0.022	-0.056	-0.026	-0.006	0.035
	Mean(after-before)	0.118	0.035	-0.135	-0.087	0.041	0.019
	P-value	0.000	0.160	0.000	0.000	0.201	0.691
F3(5)	Mean (pre-heading)	-0.009	-0.074	-0.041	-0.034	-0.035	-0.012
	Mean(post-heading)	-0.030	-0.052	0.000	0.018	-0.010	0.065
	Mean(after-before)	-0.021	0.022	0.041	0.052	0.024	0.077
	P-value	0.389	0.469	0.134	0.117	0.485	0.041
F3(6)	Mean (pre-heading)	-0.039	0.011	0.089	0.055	-0.010	0.055
	Mean(post-heading)	0.046	0.016	0.026	-0.044	0.025	0.074
	Mean(after-before)	0.085	0.005	-0.064	-0.099	0.035	0.020
	P-value	0.024	0.905	0.225	0.040	0.376	0.739
F3(7)	Mean (pre-heading)	0.004	-0.069	-0.068	-0.053	-0.036	0.011
	Mean(post-heading)	-0.012	-0.004	0.017	0.048	-0.025	0.089
	Mean(after-before)	-0.015	0.065	0.086	0.101	0.012	0.078
	P-value	0.757	0.089	0.085	0.021	0.806	0.229
F3(8)	Mean (pre-heading)	-0.061	-0.012	0.007	0.041	0.047	0.082
	Mean(post-heading)	0.001	0.036	0.047	-0.048	0.044	0.149
	Mean(after-before)	0.062	0.048	0.039	-0.089	-0.002	0.068
	P-value	0.099	0.243	0.315	0.007	0.961	0.401

Alpha							
Electrode Location	Statistics	4 rad/s			7 rad/s		
		Front Loading	Left Loading	Right Loading	Front Loading	Left Loading	Right Loading
F3(1)	Mean (pre-heading)	-0.008	0.002	-0.014	0.009	0.005	0.027
	Mean(post-heading)	0.021	-0.015	0.010	0.015	-0.004	0.033
	Mean(after-before)	0.029	-0.017	0.024	0.006	-0.010	0.006
	P-value	0.099	0.378	0.303	0.798	0.657	0.799
F3(2)	Mean (pre-heading)	0.001	-0.008	0.021	0.018	-0.003	0.003
	Mean(post-heading)	0.020	-0.028	-0.025	0.025	0.020	-0.020
	Mean(after-before)	0.019	-0.020	-0.046	0.007	0.024	-0.023
	P-value	0.226	0.355	0.003	0.733	0.342	0.263
F3(3)	Mean (pre-heading)	0.006	0.012	0.051	0.043	0.006	0.037
	Mean(post-heading)	0.000	-0.007	0.021	-0.007	0.003	0.000
	Mean(after-before)	-0.006	-0.019	-0.031	-0.051	-0.003	-0.037
	P-value	0.635	0.360	0.031	0.003	0.873	0.088
F3(4)	Mean (pre-heading)	-0.064	-0.063	-0.082	0.017	-0.043	0.062
	Mean(post-heading)	-0.052	-0.052	-0.002	-0.015	-0.024	-0.039
	Mean(after-before)	0.011	0.011	0.080	-0.033	0.019	-0.101
	P-value	0.651	0.593	0.016	0.318	0.486	0.008
F3(5)	Mean (pre-heading)	0.028	0.013	0.009	0.022	-0.005	-0.008
	Mean(post-heading)	0.004	-0.031	0.031	-0.009	0.003	0.020
	Mean(after-before)	-0.024	-0.043	0.022	-0.031	0.009	0.028
	P-value	0.274	0.138	0.213	0.248	0.806	0.266
F3(6)	Mean (pre-heading)	-0.021	0.015	0.012	0.037	-0.011	0.094
	Mean(post-heading)	0.013	0.040	0.039	0.014	0.073	-0.010
	Mean(after-before)	0.034	0.025	0.027	-0.023	0.083	-0.104
	P-value	0.174	0.644	0.508	0.552	0.027	0.038
F3(7)	Mean (pre-heading)	0.033	0.032	0.059	0.031	-0.004	-0.002
	Mean(post-heading)	0.027	-0.036	0.033	0.016	-0.009	-0.008
	Mean(after-before)	-0.007	-0.068	-0.026	-0.015	-0.004	-0.006
	P-value	0.827	0.100	0.477	0.763	0.931	0.908
F3(8)	Mean (pre-heading)	-0.018	0.055	0.028	0.051	0.001	0.076
	Mean(post-heading)	-0.058	0.003	0.064	0.010	0.083	-0.005
	Mean(after-before)	-0.040	-0.052	0.037	-0.041	0.082	-0.082
	P-value	0.288	0.365	0.306	0.226	0.101	0.129

Beta							
Electrode Location	Statistics	4 rad/s			7 rad/s		
		Front Loading	Left Loading	Right Loading	Front Loading	Left Loading	Right Loading
F3(1)	Mean (pre-heading)	0.001	-0.013	0.004	0.015	-0.017	-0.007
	Mean(post-heading)	0.005	-0.006	0.005	0.004	-0.007	-0.003
	Mean(after-before)	0.004	0.007	0.001	-0.011	0.010	0.004
	P-value	0.789	0.668	0.959	0.568	0.547	0.809
F3(2)	Mean (pre-heading)	0.005	-0.007	0.013	-0.013	-0.012	0.005
	Mean(post-heading)	0.000	-0.017	0.011	0.002	-0.014	0.016
	Mean(after-before)	-0.004	-0.009	-0.003	0.016	-0.002	0.011
	P-value	0.808	0.571	0.871	0.343	0.918	0.541
F3(3)	Mean (pre-heading)	0.022	-0.004	0.014	-0.006	-0.014	-0.017
	Mean(post-heading)	-0.013	-0.013	0.000	-0.006	-0.003	-0.013
	Mean(after-before)	-0.035	-0.009	-0.014	0.000	0.011	0.004
	P-value	0.007	0.553	0.283	0.991	0.375	0.760
F3(4)	Mean (pre-heading)	-0.064	0.033	-0.064	0.013	0.003	-0.027
	Mean(post-heading)	-0.040	-0.010	0.005	0.076	0.023	-0.032
	Mean(after-before)	0.024	-0.043	0.069	0.063	0.020	-0.005
	P-value	0.054	0.042	0.009	0.004	0.325	0.854
F3(5)	Mean (pre-heading)	0.028	-0.051	0.035	-0.048	-0.006	-0.011
	Mean(post-heading)	-0.020	-0.030	0.027	0.002	0.000	0.007
	Mean(after-before)	-0.048	0.022	-0.009	0.051	0.006	0.018
	P-value	0.013	0.380	0.678	0.001	0.753	0.398
F3(6)	Mean (pre-heading)	-0.022	-0.014	-0.034	0.052	0.003	-0.032
	Mean(post-heading)	-0.005	0.032	-0.001	0.064	-0.004	-0.018
	Mean(after-before)	0.016	0.046	0.033	0.013	-0.006	0.014
	P-value	0.602	0.126	0.382	0.773	0.808	0.752
F3(7)	Mean (pre-heading)	0.042	-0.071	0.042	-0.014	-0.024	-0.035
	Mean(post-heading)	0.000	-0.046	0.033	-0.028	-0.024	0.033
	Mean(after-before)	-0.042	0.025	-0.009	-0.014	0.001	0.068
	P-value	0.226	0.583	0.784	0.616	0.980	0.034
F3(8)	Mean (pre-heading)	0.020	-0.012	-0.027	-0.013	-0.022	-0.022
	Mean(post-heading)	-0.023	0.060	-0.019	0.030	0.028	-0.039
	Mean(after-before)	-0.042	0.072	0.008	0.043	0.050	-0.018
	P-value	0.160	0.022	0.784	0.193	0.081	0.635

Gamma							
Electrode Location	Statistics	4 rad/s			7 rad/s		
		Front Loading	Left Loading	Right Loading	Front Loading	Left Loading	Right Loading
F3(1)	Mean (pre-heading)	0.008	-0.009	-0.002	0.006	-0.003	0.015
	Mean(post-heading)	0.004	0.015	0.002	-0.004	-0.012	0.004
	Mean(after-before)	-0.003	0.024	0.004	-0.010	-0.009	-0.010
	P-value	0.706	0.007	0.796	0.452	0.568	0.457
F3(2)	Mean (pre-heading)	-0.012	-0.007	0.005	0.011	0.001	-0.005
	Mean(post-heading)	-0.007	-0.007	0.010	0.002	-0.012	-0.002
	Mean(after-before)	0.005	-0.001	0.005	-0.009	-0.013	0.003
	P-value	0.535	0.944	0.595	0.496	0.299	0.787
F3(3)	Mean (pre-heading)	-0.009	-0.010	-0.011	-0.014	-0.006	-0.005
	Mean(post-heading)	0.008	-0.006	-0.001	0.001	-0.007	0.016
	Mean(after-before)	0.017	0.003	0.011	0.014	-0.001	0.021
	P-value	0.055	0.703	0.215	0.123	0.952	0.034
F3(4)	Mean (pre-heading)	-0.025	-0.045	-0.034	0.002	-0.034	-0.022
	Mean(post-heading)	-0.002	-0.042	-0.041	-0.006	-0.001	0.014
	Mean(after-before)	0.023	0.003	-0.006	-0.007	0.033	0.035
	P-value	0.024	0.810	0.722	0.666	0.165	0.040
F3(5)	Mean (pre-heading)	-0.014	-0.023	0.011	0.026	-0.007	-0.009
	Mean(post-heading)	-0.014	-0.026	0.013	-0.014	-0.022	-0.003
	Mean(after-before)	0.000	-0.003	0.002	-0.040	-0.015	0.006
	P-value	0.991	0.812	0.909	0.027	0.442	0.629
F3(6)	Mean (pre-heading)	-0.008	-0.032	-0.028	-0.014	0.005	-0.034
	Mean(post-heading)	0.019	-0.039	-0.029	0.000	0.019	0.011
	Mean(after-before)	0.027	-0.007	-0.002	0.014	0.014	0.045
	P-value	0.249	0.760	0.943	0.525	0.707	0.023
F3(7)	Mean (pre-heading)	-0.013	-0.018	0.034	0.041	-0.013	-0.014
	Mean(post-heading)	-0.007	-0.013	0.001	-0.023	-0.056	0.010
	Mean(after-before)	0.006	0.005	-0.032	-0.064	-0.043	0.024
	P-value	0.711	0.818	0.347	0.040	0.112	0.149
F3(8)	Mean (pre-heading)	-0.023	0.006	-0.032	-0.026	-0.005	-0.042
	Mean(post-heading)	0.006	-0.024	-0.014	0.001	0.017	0.032
	Mean(after-before)	0.030	-0.030	0.018	0.027	0.022	0.074
	P-value	0.334	0.213	0.320	0.146	0.515	0.007

Appendix B: Summary Statistics of the Heading Data

Table 6.1 Summary statistics of the whole data of change in absolute power from pre-heading to post-heading

Statistics	Frequency Band					
	Delta	Theta	Alpha	Beta	Gamma	Total
Minimum	-5205.774	-907.934	-64.687	-260.350	-25.425	-2803.275
1st Quartile	-0.177	-0.250	-0.318	-0.959	-0.084	-0.132
Median	0.156	0.109	0.006	0.873	0.169	0.124
Mean	-0.454	0.487	0.755	5.335	1.352	-0.849
3rd Quartile	1.259	0.719	0.707	4.823	1.337	1.063
Maximum	607.961	242.691	105.052	399.920	63.390	112.084
N	912	912	912	912	912	912

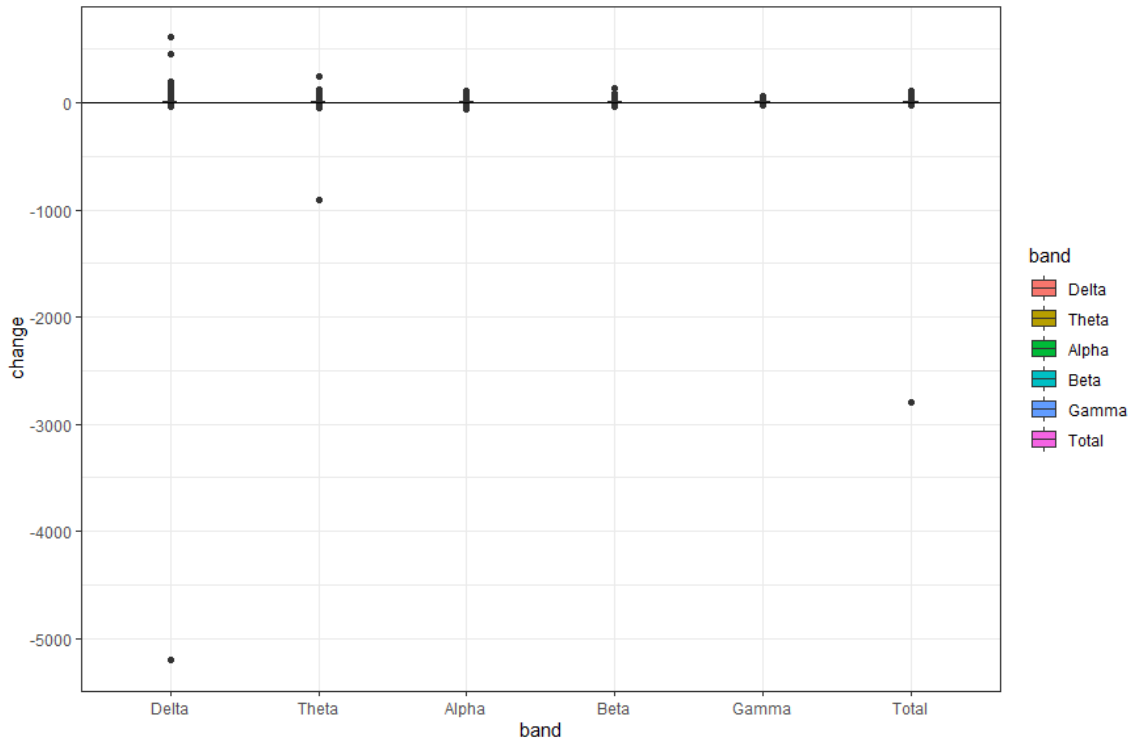

Figure 6.1 Boxplot of change in absolute power from pre-heading to post-heading for the whole data of absolute power

Table 6.2 Summary statistics of the trimmed data of change in absolute power from pre-heading to post-heading

Statistics	Frequency Band					
	Delta	Theta	Alpha	Beta	Gamma	Total
Minimum	-38.448	-29.979	-64.686	-109.220	-21.982	-22.346
1st Quartile	-0.104	-0.308	-0.347	-0.937	-0.078	-0.080
Median	0.129	0.071	0.012	0.747	0.167	0.141
Mean	9.761	1.202	0.977	6.620	0.985	5.520
3rd Quartile	1.265	0.600	0.840	5.329	0.776	1.210
Maximum	398.171	242.692	105.050	399.906	63.391	214.256
N	912	912	912	912	912	912

Table 6.3 Summary statistics of the data of change in relative power from pre-heading to post-heading

Statistics	Frequency Band				
	Delta	Theta	Alpha	Beta	Gamma
Minimum	-33.24%	-26.18%	-30.72%	-30.64%	-27.87%
1st Quartile	-4.40%	-6.24%	-8.15%	-4.37%	-5.17%
Median	3.60%	-1.23%	-2.31%	-0.51%	-0.90%
Mean	6.69%	-2.21%	-2.67%	-1.42%	-1.38%
3rd Quartile	14.33%	2.98%	2.19%	2.25%	2.99%
Maximum	69.63%	17.61%	30.59%	15.88%	23.21%
N	912	912	912	912	912

Table 6.4 Summary statistics of magnitude squared coherence data

Statistics	Frequency Band				
	Delta	Theta	Alpha	Beta	Gamma
Minimum	-0.619	-0.385	-0.330	-0.381	-0.320
1st Quartile	-0.100	-0.075	-0.059	-0.048	-0.045
Median	-0.007	-0.015	0.001	0.004	0.000
Mean	-0.003	-0.016	0.004	0.005	-0.004
3rd Quartile	0.087	0.039	0.064	0.056	0.044
Maximum	0.603	0.385	0.435	0.353	0.350
N	1786	1786	1786	1786	1786

Table 6.5 Summary statistics of imaginary coherence data

Statistics	Frequency Band				
	Delta	Theta	Alpha	Beta	Gamma
Minimum	-0.770	-0.674	-0.596	-0.398	-0.338
1st Quartile	-0.104	-0.094	-0.108	-0.079	-0.048
Median	0.005	0.009	-0.006	0.002	0.008
Mean	0.007	0.012	-0.010	0.003	0.004
3rd Quartile	0.123	0.120	0.094	0.087	0.060
Maximum	0.636	0.681	0.619	0.402	0.376